



Metabolomic Detection Between Pancreatic Cancer and Liver Metastasis Nude Mouse Models Constructed by Using the PANC1-KAI1/CD₈₂ Cell Line

Technology in Cancer Research & Treatment
Volume 20: 1-21
© The Author(s) 2021
Article reuse guidelines:
sagepub.com/journals-permissions
DOI: 10.1177/15330338211045204
journals.sagepub.com/home/tct


Shuo Wang, PhD¹, Jiang Chen, PhD¹, Hongyu Li, PhD¹,
Xingshun Qi, PhD¹, Xu Liu, PhD¹, and Xiaozhong Guo, PhD¹ 

Abstract

Background: Pancreatic cancer (PC) has a poor prognosis and is prone to liver metastasis. The KAI1/CD₈₂ gene inhibits PC metastasis. This study aimed to explore differential metabolites and enrich the pathways in serum samples between PC and liver metastasis nude mouse models stably expressing KAI1/CD₈₂. **Methods:** KAI1/CD₈₂-PLV-EF1 α -MCS-IRES-Puro vector and PANC1 cell line stably expressing KAI1/CD₈₂ were constructed for the first time. This cell line was used to construct 3 PC nude mouse models and 3 liver metastasis nude mouse models. The different metabolites and Kyoto encyclopedia of genes and genomes (KEGG) and human metabolome database (HMDB) enrichment pathways were analyzed using the serum samples of the 2 groups of nude mouse models on the basis of untargeted ultra-performance liquid chromatography-tandem mass spectrometry platform. **Results:** KAI1/CD₈₂-PLV-EF1 α -MCS-IRES-Puro vector and PANC1 cell line stably expressing KAI1/CD₈₂ were constructed successfully, and all nude mouse models survived and developed cancers. Among the 1233 metabolites detected, 18 metabolites (9 upregulated and 9 downregulated) showed differences. In agreement with the literature data, the most significant differences between both groups were found in the levels of bile acids (taurocholic acid, chenodeoxycholic acid), glycine, prostaglandin E₂, vitamin D, guanosine monophosphate, and inosine. Bile recreation, primary bile acid biosynthesis, and purine metabolism KEGG pathways and a series of HMDB pathways ($P < .05$) contained differential metabolites that may be associated with liver metastasis from PC. However, the importance of these metabolites on PC liver metastases remains to be elucidated. **Conclusions:** Our findings suggested that the metabolomic approach may be a useful method to detect potential biomarkers in PC.

Keywords

metabolomics, KAI1/CD₈₂, pancreatic cancer, nude mouse models, biomarker

Abbreviations

BSA, bovine serum albumin; CA19-9, carbohydrate antigen 19-9; DMEM, Dulbecco's modified eagle medium; ECL, electrochemiluminescence; FC, fold change; GMP, guanosine monophosphate; HBSS, Hank's balanced salt solution; HCA, hierarchical cluster analysis; HMDB, human metabolome database; KEGG, Kyoto encyclopedia of genes and genomes; LC-MS/MS, liquid chromatography-mass spectrometry; LDH, lactate dehydrogenase; NMR, nuclear magnetic resonance; OPLS-DA, orthogonal partial least squares discrimination analysis; PC, pancreatic cancer; PCA, principal component analysis; PCCs, Pearson correlation coefficients; PCR, polymerase chain reaction; PGE₂, prostaglandin E₂; PMSF, phenylmethylsulfonyl fluoride; PKC, protein kinase C; PVDF, polyvinylidene fluoride; SMPDB, small molecule pathway database; TBST, tris buffered saline tween; TNF- α , tumor necrosis factor- α ; TM4SF, transmembrane 4 superfamily; UPLC-MS/MS, ultra-performance liquid

General Hospital of Northern Theater Command of China Medical University, Shenyang, Liaoning Province, P.R. China

Corresponding Author:

Xiaozhong Guo, PhD, Department of Gastroenterology, General Hospital of Northern Theater Command of China Medical University, No. 83 Wenhua Road, Shenyang, 110840 Liaoning Province, China.
Email: xiaozhong_guo@126.com



Creative Commons Non Commercial CC BY-NC: This article is distributed under the terms of the Creative Commons Attribution-NonCommercial 4.0 License (<https://creativecommons.org/licenses/by-nc/4.0/>) which permits non-commercial use, reproduction and distribution of the work without further permission provided the original work is attributed as specified on the SAGE and Open Access page (<https://us.sagepub.com/en-us/nam/open-access-at-sage>).

chromatography-tandem mass spectrometry; TEMED, tetramethylethylenediamine; VEGF, vascular endothelial growth factor; VIP, variable importance in projection.

Received: January 16, 2021; Revised: August 13, 2021; Accepted: August 20, 2021.

Introduction

As one of the most aggressive malignancies, pancreatic cancer (PC) is a leading cause of cancer-related mortality.¹ More than 80% of patients with PC are at the advanced stage of initial diagnosis, losing the opportunity for surgical treatment. Moreover, the effect of radiotherapy and chemotherapy is poor.² Currently, carbohydrate antigen 19-9 (CA19-9), a common clinical biomarker for PC, does not have a sufficient ability to detect PC at an early stage.³ Imaging examination shows insufficient sensitivity and specificity when the tumor size is less than 2 cm.⁴ Direct peripancreatic invasion or metastasis to near and far organs may occur through lymph nodes and/or blood vessels. Blood from the pancreas flows back through the portal vein to the liver, which is the most common site of metastasis in PC. Therefore, new markers that can diagnose the risk of PC liver metastasis are urgently needed.

In 1995, Dong et al. first discovered the KAI1/CD₈₂ gene (named according to the Chinese anticancer compound Kang Ai),⁵ which has been shown to inhibit the metastasis of most cancers and to be significantly associated with prognosis. KAI1/CD₈₂ is a member of the transmembrane 4 superfamily. It includes 4 conservative hydrophobic domains (TM1–TM4) across the membrane structure and 1 extracellular carbohydrate binding site. Similar to other TM4SF members, this structure determines whether KAI1/CD₈₂ can influence the molecular rearrangement and cell morphology, aggregation, adhesion, and migration.⁶ The inhibitory effect of KAI1/CD₈₂ on PC was first discovered in 1996. In situ hybridization and immunohistochemical analysis showed that the KAI1/CD₈₂ protein is expressed to varying degrees in PC, but it is not or weakly expressed in the surrounding stroma, inflammatory cells, islet cells, and acinar cells in adjacent tissues.⁷ In vitro experiments demonstrated that KAI1/CD₈₂ can inhibit the metastasis of PC cells by inhibiting their movement and migration.⁶ The KAI1/CD₈₂ gene downregulates hGF-mediated infiltration and metastasis of PC cells by inhibiting SPK1 activity.⁸ KAI1/CD₈₂ also inhibits angiogenesis and lymphatic metastasis in PC by inhibiting vascular endothelial growth factor C (VEGF-C) expression.⁹ KAI1 inhibited pathological angiogenesis by regulating membrane lipid rearrangement and cell adhesion molecule CD44.¹⁰ KAI1 also inhibits tumor metastasis by inhibiting hepatocyte growth factor (HGF/c-Met) and integrin pathways.¹¹ Low expression of KAI1 that reduce intercellular adhesion leads to the occurrence of epithelial-mesenchymal transition (EMT) metastasis.¹² Considering that liver is the organ with the highest metastatic rate of PC, this study is the first to investigate the correlation between KAI1 and liver metastasis of PC. We attempted

to explore the differential metabolites and their enrichment pathways between pancreatic carcinoma in situ and liver metastasis from a new perspective of metabolomics. The molecular regulatory network of KAI1/CD₈₂ to inhibit pancreatic tumor metastasis needs to be fully elucidated so as to provide a new way for diagnosing and treating PC patients.

Metabolomics is an analysis of endogenous low-molecular-weight metabolites present in a defined biological sample such as tissue or a bodily fluid such as blood.^{13–15} Metabolomics has attracted increasing interest in the scientific and medical communities in the past few years, particularly in oncology.¹⁶ Compared with normal differentiated cells, cancer cells have considerably different metabolic requirements that enable them to continuously grow. Thus, cancer cells must have altered metabolic pathways to obtain sufficient amounts of the metabolites required for high rates of proliferation.¹⁷ Small effective changes in gene and protein expression will be amplified on metabolites, and the biochemical metabolic network of many endogenous small-molecule compounds is relatively clear. As a new metabolomic analysis technique, liquid chromatography–mass spectrometry (LC-MS/MS) has high sensitivity and wide dynamic range and does not require derivatization. It is suitable for detecting substances with large polarity and molecular weight, such as lipids, nucleotides, and polyamines. In recent years, LC-MS/MS has been utilized to explore the metabolic processes and new diagnostic biomarkers for early diagnosis in various cancers, including PC. In some studies, the LC-MS/MS platform used untargeted metabolomics to distinguish PC from noncancer controls,^{18–20} including 1 diabetes cohort²¹ and 1 pancreatitis cohort.²² Other studies utilized targeted metabolomics.^{23–25} These selected individual biomarkers can be used to detect PC, with an area under curve (AUC) >0.8.^{19–21,25}

The present study aimed to discover different metabolites and metabolic pathways in carcinoma in situ of the pancreas and liver metastasis using serum samples and then identify new targets for the anticancer mechanism of the KAI1/CD₈₂ gene. To our knowledge, this study was the first to create cell lines stably expressing KAI1/CD₈₂. The PC in situ and liver metastasis models were constructed by using the human PC cell line PANC-1 and administered in nude mice via splenic injection. In this study, 6 serum samples were utilized, and 1223 metabolites were detected by full-spectrum metabolome detection based on extensive targeting technology. On the basis of UPLC-MS/MS detection platform, self-built database, and multivariate statistical analysis, metabolic group differences among samples were studied. Some different metabolites and pathways were screened out to predict and analyze the related functions of the metabolites in the samples.

Materials and Methods

Ethics Approval

All methods aimed to minimize the suffering of experimental animals were performed in accordance with the animal ethics guidelines and approved by the Ethics Board of China Medical University. The approval number of this animal research was IACUC-001-13.

Cell Lines and Experimental Animals

PANC-1, human PC cell lines, were ordered from the Institute of Cell Biology of Chinese Academy of Sciences. The cells were cultured in Dulbecco's modified eagle's medium (DMEM), which was supplemented with 10% fetal bovine serum, L-glutamine (2 mmol/L), penicillin G (100 U/mL), and streptomycin (0.1 mg/mL) in an incubator (37 °C, 5% CO₂, and 95% humidity). The experimental animals were female BALB/c nude mice aged 4 to 6 weeks and weighing 18 to 22 g. Facilities: SPF barrier environment and IVC cage feeding. Feed: Pellet feed, Jiangsu Synergetic Pharmaceutical Bioengineering Co., Ltd. Drinking water: Sterile water. Feeding density: 6 animals per cage. Cage change frequency: twice a week. Fasting: N/A. Special feeding: N/A. Rich environment: make nest paper or toys.

Reagents and Equipment

The reagents used were as follows: Acetonitrile (Merck KGaA); 30% Acr-Bos (29:1) (Biyuntian); Anti- β Actin antibodies (Abcam ab8226 1:2000); Anti-CD82 antibodies (Abcam ab109529 1:1000); Ammonium formate (Thermo Fisher); Ammonium persulfate (Merck KGaA); BCA test kit (Biyuntian); Bovine serum albumin (LABLEAD); Dichloromethane (Thermo Fisher); DMEM (GE Healthcare Life Sciences); Electrochemiluminescence (ECL) (Thermo Fisher); ExoIII Buffer (Thermo Fisher); Fast Digest Buffer, Fast Digest xhoI, Fast Digest HindIII (Thermo Fisher); Formic acid (Merck KGaA); Gel Recovery Kit 28706 (QIAGEN); Goat anti-rabbit IgG (Thermo 31340 1:100 000-1:200 000) and Goat anti-rabbit IgG (Thermo 31460 1:100 000-1:200 000) (Thermo Fisher); Isopropyl alcohol (Merck KGaA); Lipofectamin 2000 (Thermo Fisher); Loading Buffer (Biyuntian); Methanol (Merck KGaA); Methyl tert-butyl ether (Merck KGaA); Tetramethylethylenediamine (Merck KGaA); Opti-MEM (Thermo Fisher); Phenylmethylsulfonyl fluoride (Biyuntian); Polyvinylidene fluoride (PVDF) membrane (Millipore); Standard reagent 12:0 Lyso PC, Cer(d18:1/4:0), PC (13:0/13:0), DG (12:0/12:0), TG (17:0/17:0/17:0) (Avanti/zzstandard); Tris-HCl, PH8.8 (Biyuntian), Tris-HCl, PH6.8 (Biyuntian); Total protein extraction kit (Biyuntian).

The equipments used were as follows: Ball mill instrument (MM400) (Retsch); Centrifugal concentrator (CentriVap); Centrifuge (5424R) (Eppendorf); Electronic balance (AS 60/220.R2) (RADWAG); Full wavelength scanning multifunction

reading instrument (Thermo Fisher); HH.SII-1 Thermostat water bath (Chang'an Scientific Instrument Factory); LC-MS/MS (ExionLC AD UPLC-QTRAP) (SCIEX); Tanon EPS 300 Electrophoresis apparatus (Tianeng Technology Co., Ltd); TGL-16G Table High Speed Centrifuge (Sihuan Scientific Instrument Factory); Ultrasonic cleaning apparatus (KQ5200E) (Kunshan Ultrasonic Instrument Co., Ltd); Vortex mixer (VORTEX-5) (Kyllin-Bell); TGL-16G Table High Speed Centrifuge (Sihuan Scientific Instrument Factory).

PANC1-KAI1 Cell Line

The KAI1-PLV-EF1 α -MCS-IRES-Puro vector was first constructed. The target gene fragment was amplified and purified by polymerase chain reaction (PCR) (reaction system: 50-100 mg of template, 2 μ L of primer-F, 2 μ L of primer-R, 25 μ L of primer-STAR, deionized water to reach a volume of 50 μ L; response procedures: 98 °C for 10 s, 55 °C for 15 s, 72 °C for 1 kb/min with 30 cycles). The PLV-EF1 α -MCS-IRES-Puro vector was double-digested by Thermo Scientific FastDigest XhoI and Thermo Scientific FastDigest HindIII. Exonuclease III was used to connect the skeleton vector and the target fragment to construct the recombinant plasmid for transformation. PCR amplification of the KAI1/CD₈₂-PLV-EF1 α -MCS-IRES-Puro vector was detected by agarose gel electrophoresis.

Then, we constructed the PANC1 cell line stably expressing KAI1/CD₈₂. The KAI1-PLV-EF1 α -MCS-IRES-Puro vector was cotransfected with virus-packed plasmid pMDLg/pRRE, VSV-G, and pRSV-Rev into HEK293T cells using Lipofectamine 2000. The cells were cultured and collected after 48 and 72 h. PANC1 cells were infected after the 2 supernatants were mixed (the cell adherence rate was 70%). The number of positive fluorescent signals in cells was detected by flow cytometry to determine the infection rate of PANC1 cells by green fluorescent protein. Puro antibiotics (5 μ g/mL) were added into monoclonal cells for screening. The expression of the KAI1/CD₈₂ protein was confirmed by Western blot.

Nude Mouse Xenograft Model

PC Nude Mouse Model. The PANC1-KAI1/CD₈₂ cell line digested by trypsin was suspended with Hank's balanced salt solution (HBSS). The cell suspension of each strain was collected and cultured at a concentration of 1×10^7 cells/mL and was inoculated in situ into the pancreas of nude mice with 0.1 mL of each cell. Successful injection was indicated by the presence of liquid blisters under the subcapsular region of the pancreas without any liquid exposure, and the abdominal wound was sutured. The principle of aseptic operation should be strictly observed during the surgical operation. After waking up under anesthesia, the mice were placed in an SPF grade feeding chamber. After 5 weeks, the mice were sacrificed, and their serum samples were collected and measured.

Nude Mouse Model of Splenic Injection Liver Metastasis. The PANC1-KAI1/CD₈₂ cell line digested by trypsin was suspended with HBSS. The cell suspension of each strain was collected and cultured at a concentration of 1×10^7 cells/mL and was inoculated into the spleen of nude mice with 0.1 mL of each cell. After injection, a 75% alcohol cotton ball was used to compress the pinhole for 1 to 2 min. Care was taken to stop bleeding in order to prevent cancer cell extravasation and implantation metastasis in the abdominal cavity. Subsequently, the wound was sutured. Successful injection was marked by subcapsular fluid blisters and no fluid exposure. The principle of aseptic operation should be strictly observed during the surgical operation. After waking up under anesthesia, the mice were placed in an SPF grade feeding chamber. After 5 weeks, the mice were sacrificed, and their serum samples were collected and measured.

Blood Sample Extraction

Methods for extraction of hydrophilic compounds. The sample was thawed on ice, vortexed for 10 s, and mixed well. About 300 μ L of pure methanol was added to 50 μ L of serum. The mixture was vortexed for 3 min and centrifuged at 12 000 rpm at 4 °C for 10 min. Then, the supernatant was collected and centrifuged at 12 000 rpm at 4 °C for 5 min. The sample was placed in a refrigerator at -20 °C for 30 min and then centrifuged at 12 000 rpm at 4 °C for 3 min. Finally, 150 μ L of the supernatant in the liner of the corresponding injection bottle was taken for on-board analysis.

Methods for extraction of hydrophobic compounds. The sample was thawed on ice, vortexed for 10 s, and then centrifuged at 3000 rpm at 4 °C for 5 min. About 50 μ L of 1 sample was taken and homogenized with 1 mL mixture comprising methanol, MTBE, and internal standard mixture. The mixture was vortexed for 15 min. Then, 200 μ L of water was added, and the mixture was vortexed for 1 min and centrifuged at 12 000 rpm at 4 °C for 10 min. About 500 μ L of supernatant was extracted and concentrated. The powder was dissolved with 200 μ L of mobile phase B and then stored at -80 °C. Finally, the dissolving solution was transferred into the sample bottle for LC-MS/MS analysis.

UPLC Conditions

UPLC Conditions of Hydrophilic Compounds. The sample extracts were analyzed using an LC-ESI-MS/MS system (UPLC, ExionLC AD, <https://sciex.com.cn/>; MS, QTRAP® System, <https://sciex.com/>). The analytical conditions were as follows: UPLC: column, Waters ACQUITY UPLC HSS T3 C18 (1.8 μ m, 2.1 mm \times 100 mm); column temperature, 40 °C; flow rate, 0.4 mL/min; injection volume, 2 μ L; solvent system, water (0.1% formic acid): acetonitrile (0.1% formic acid); gradient program, 95:5 V/V at 0 min, 10:90 V/V at 11.0 min,

10:90 V/V at 12.0 min, 95:5 V/V at 12.1 min, and 95:5 V/V at 14.0 min.

UPLC Conditions of Hydrophobic Compounds. The sample extracts were analyzed using an LC-ESI-MS/MS system (UPLC, ExionLC AD, <https://sciex.com.cn/>; MS, QTRAP® System, <https://sciex.com/>). The analytical conditions were as follows: UPLC: column, Thermo Accucore™ C30 (2.6 μ m, 2.1 mm \times 100 mm i.d.); solvent system, A: acetonitrile/water (60/40, V/V, 0.1% formic acid, 10 mmol/L ammonium formate), B: acetonitrile/isopropanol (10/90 V/V, 0.1% formic acid, 10 mmol/L ammonium formate); gradient program, A/B (80:20, V/V) at 0 min, 70:30 V/V at 2.0 min, 40:60 V/V at 4 min, 15:85 V/V at 9 min, 10:90 V/V at 14 min, 5:95 V/V at 15.5 min, 5:95 V/V at 17.3 min, 80:20 V/V at 17.3 min, 80:20 V/V at 20 min; flow rate, 0.35 mL/min; temperature, 45 °C; injection volume: 2 μ L. The effluent was alternatively connected to an ESI-triple quadrupole-linear ion trap (QTRAP)-MS.

ESI-Q TRAP-MS/MS

ESI-Q TRAP-MS/MS of Hydrophilic Compounds. LIT and triple quadrupole (QQQ) scans were acquired on a triple quadrupole-linear ion trap mass spectrometer (QTRAP, QTRAP® LC-MS/MS System) equipped with an ESI TurboIonSpray interface, operating in positive and negative ion mode, and controlled by Analyst 1.6.3 software (Sciex). The ESI source operation parameters were as follows: source temperature 500 °C; ion spray voltage (IS) 5500 V (positive), -4500 V (negative); ion source gas I (GSI), gas II (GSII), and curtain gas (CUR) were set at 55, 60, and 25.0 psi, respectively; the collision gas (CAD) was high. Instrument tuning and mass calibration were performed with 10 and 100 μ mol/L polypropylene glycol solutions in QQQ and LIT modes, respectively. A specific set of MRM transitions was monitored for each period according to the metabolites eluted within this period.

ESI-Q TRAP-MS/MS of Hydrophobic Compounds. LIT and QQQ scans were acquired on a QTRAP® LC-MS/MS System equipped with an ESI TurboIonSpray interface, operating in positive and negative ion mode, and controlled by Analyst 1.6.3 software (Sciex). The ESI source operation parameters were as follows: ion source, turbo spray; source temperature 500 °C; ion spray voltage (IS) 5500 V(positive), -4500 V(negative); ion source gas 1 (GS1), gas 2 (GS2), and curtain gas (CUR) were set at 45, 55, and 35 psi, respectively; the collision gas (CAD) was medium. Instrument tuning and mass calibration were performed with 10 and 100 μ mol/L polypropylene glycol solutions in QQQ and LIT modes, respectively. QQQ scans were acquired as MRM experiments with collision gas (nitrogen) set to 5 psi. DP and CE for individual MRM transitions were performed with further DP and CE optimization. A specific set of MRM transitions was monitored for each period according to the metabolites eluted within this period.

Data Analysis

Principal Component Analysis. Unsupervised principal component analysis (PCA) was performed by statistics function `prcomp` within R (www.r-project.org). The data were unit variance scaled before unsupervised PCA.

Hierarchical Cluster Analysis and Pearson Correlation Coefficients.

The hierarchical cluster analysis (HCA) results of samples and metabolites were presented as heatmaps with dendrograms, whereas the Pearson correlation coefficients (PCCs) between samples were calculated by the `cor` function in R and presented only as heatmaps. Both HCA and PCC were carried out by R package `ComplexHeatmap`. For HCA, the normalized signal intensities of metabolites (unit variance scaling) were visualized as a color spectrum.

Selection of Differential Metabolites. The significantly regulated metabolites between groups were determined by variable importance in projection (VIP) ≥ 1 and absolute Log_2^{FC} (fold change) ≥ 1 . VIP values were extracted from orthogonal partial least squares discrimination analysis (OPLS-DA) result, which also contain score plots and permutation plots, generated using R package `MetaboAnalystR`. The data were log transformed (\log_2) and subjected to mean centering before OPLS-DA. A permutation test (200 permutations) was performed to avoid overfitting.

Kyoto Encyclopedia of Genes and Genomes Annotation and Enrichment Analysis. The identified metabolites were annotated using Kyoto encyclopedia of genes and genomes (KEGG) compound database (<http://www.kegg.jp/kegg/compound/>). The annotated metabolites were then mapped to the KEGG Pathway database (<http://www.kegg.jp/kegg/pathway.html>). Significantly enriched pathways were identified with a hypergeometric test's *P*-value for a given list of metabolites.

Western Blot

First, 10% separation gel and 4% stacking gel were configured. Second, 5 to 20 μg of protein were loaded. When the strip was pressed into a line and reached the junction between the separation gel and the stacking gel, the voltage was adjusted to 110 V until the electrophoresis ended. Third, a PVDF membrane was cut according to the length of the sample. The PVDF membrane was activated in 100% methanol solution for 10 s and then balanced in the electrotransfer solution for 5 min. It is generally transferred by 300 mA for 1 to 3 h. Fourth, 5% skimmed milk was used for sealing for 1 h. Goat anti-rabbit IgG (Thermo 31340) was added: 1% to 5% skim milk powder or tris buffered saline tween (TBST) with diluted primary antibody, incubate overnight at 4 °C, and wash with TBST for 3 times (10 min each time). Goat anti-rabbit IgG (Thermo 31460) was added: 1% to 5% skim milk powder or TBST with diluted secondary antibody (1:100 000-1:200 000),

incubate at room temperature for 1 h, and wash with TBST for 3 times (10 min each time). Finally, ECL was evenly added on the PVDF membrane and gelatinized for several seconds after the reaction.

Results

PANC1-KAI1 Cell Line

The PCR identification results of KAI1/CD₈₂ PLV-EF1 α -positive bacterial solution are shown in Figure 1a. The efficiency of PANC1 cell lentivirus infection is shown in Figure 1b. The KAI1/CD₈₂ overexpression and Western blot results of stable conversion of PANC1 cell line are shown in Figure 1c and d. The Western blot results showed that the monoclonal cells after virus infection could stably overexpress KAI1/CD₈₂ after screening, which proved that the stable cell line had been successfully constructed. P12 cells had poor resuscitation; thus, P16 was finally selected for subsequent experiments.

Nude Mouse Xenograft Models

Three PC nude mouse models and 3 splenic injection liver metastasis nude mouse models survived and developed cancers (Figure 1e and f).

UPLC-MS/MS-Based Full spectrum Metabolomics

Six serum samples of the 2 groups were used for full spectrum metabolomic analysis based on UPLC-MS/MS platform, including 3 KAI1/CD₈₂-PC nude mouse models and 3 KAI1/CD₈₂-liver metastasis nude mouse models. The flow chart of analysis is shown in Figure 2.

Statistical Analysis of Differentially Expressed Metabolites. PCA and OPLS-DA were utilized to evaluate the differences in the expression of tissue metabolites between groups. PCA is a multidimensional data statistical analysis method for unsupervised pattern recognition. A set of potentially correlated variables are converted into a set of linearly uncorrelated variables through orthogonal transformation. The converted variables are called principal components. PCA data processing principle: the original data is compressed into *N* principal components to describe the features of the original data set, PC1 represents the most obvious features in the multidimensional data matrix, PC2 represents the most significant features in the data matrix except PC1, PC3, ..., PC*N*, and so on. PCA uses the built-in statistical `PRCOMP` function of R software (www.r-project.org/) and sets the `PRCOMP` function parameter `scale = True` to represent the normalization of unit variance scaling on the data. PCA was performed on the samples (including the quality control samples) in order to preliminarily understand the total metabolic differences between the samples of each group and the degree of variation between the samples within the group. PCA results showed the tendency of metabolome separation among each group, indicating whether

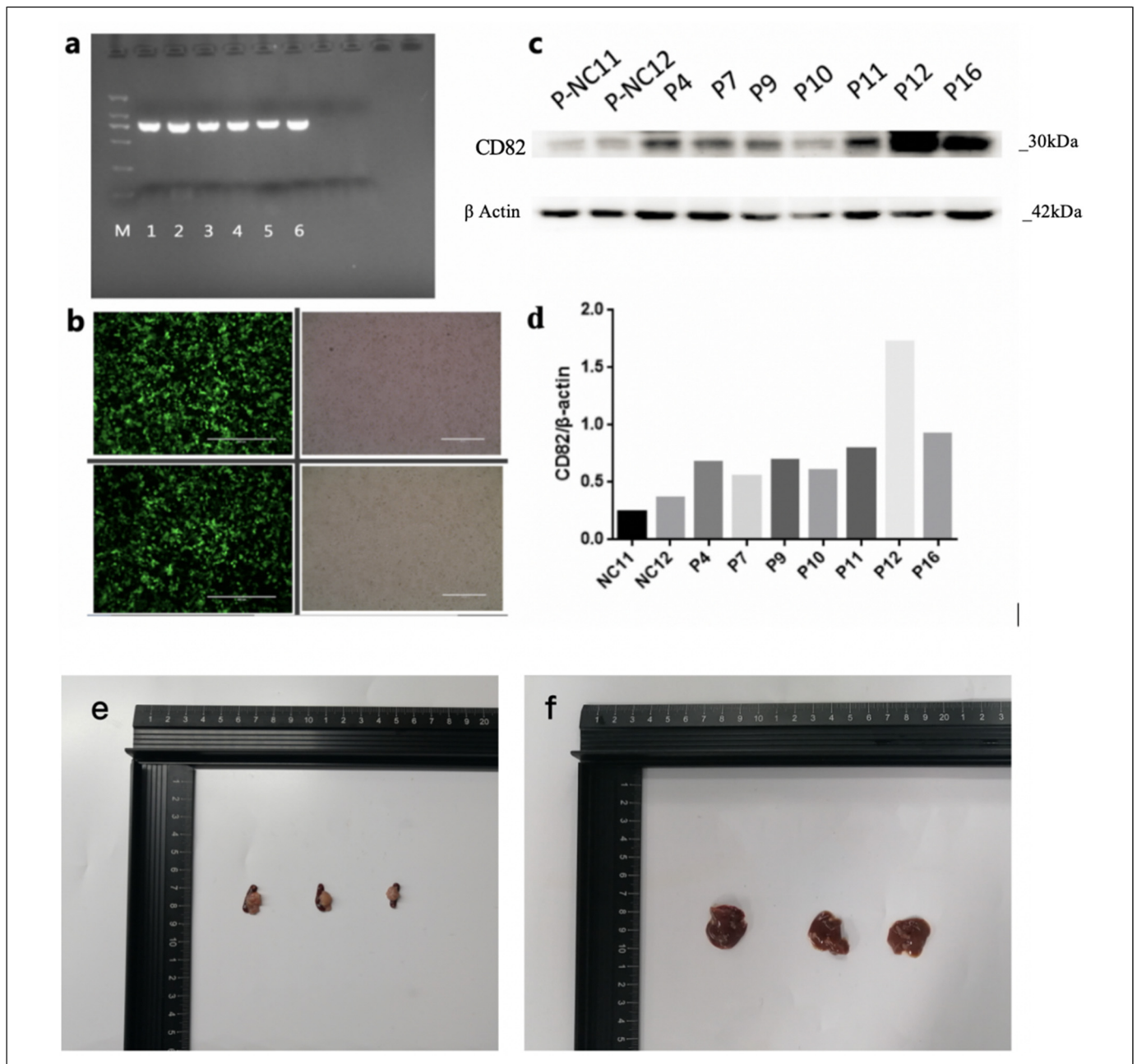


Figure 1. Lentivirus packaging and nude mouse xenograft models. (a) Polymerase chain reaction (PCR) identification results of KAI1/CD₈₂ PLV-EF1 α -positive bacterial solution. (b) Efficiency of PANC1 cell lentivirus infection. (c and d) Western blot of KAI1/CD₈₂ protein expression. (e) Three PC tissues of nude mouse models. (f) Three liver metastasis tissues of nude mouse models.

there was difference in metabolome between sample groups. PCA showed distinct clustering between different groups (Figure 3a to c), respectively. Although PCA is effective in extracting the main information, it is insensitive to the variables with small correlation which can be solved by partial least squares discriminant analysis (PLS-DA). PLS-DA is a multivariate statistical analysis method with supervised pattern recognition. Specifically, the components in independent variable X and dependent variable Y are extracted, respectively, and then the correlation between the

components is calculated. Compared with PCA, PLS-DA can maximize the differentiation between groups and is conducive to the search for differential metabolites. Orthogonal partial least squares discriminant analysis (OPLS-DA) combines the orthogonal signal correction and PLS-DA methods, which can decompose the information of X matrix into 2 kinds of information related to Y and unrelated to Y and screen the difference variables by removing the unrelated differences. The OPLS-DA score plot and OPLS-DA model validation are shown in Figure 4a and b.

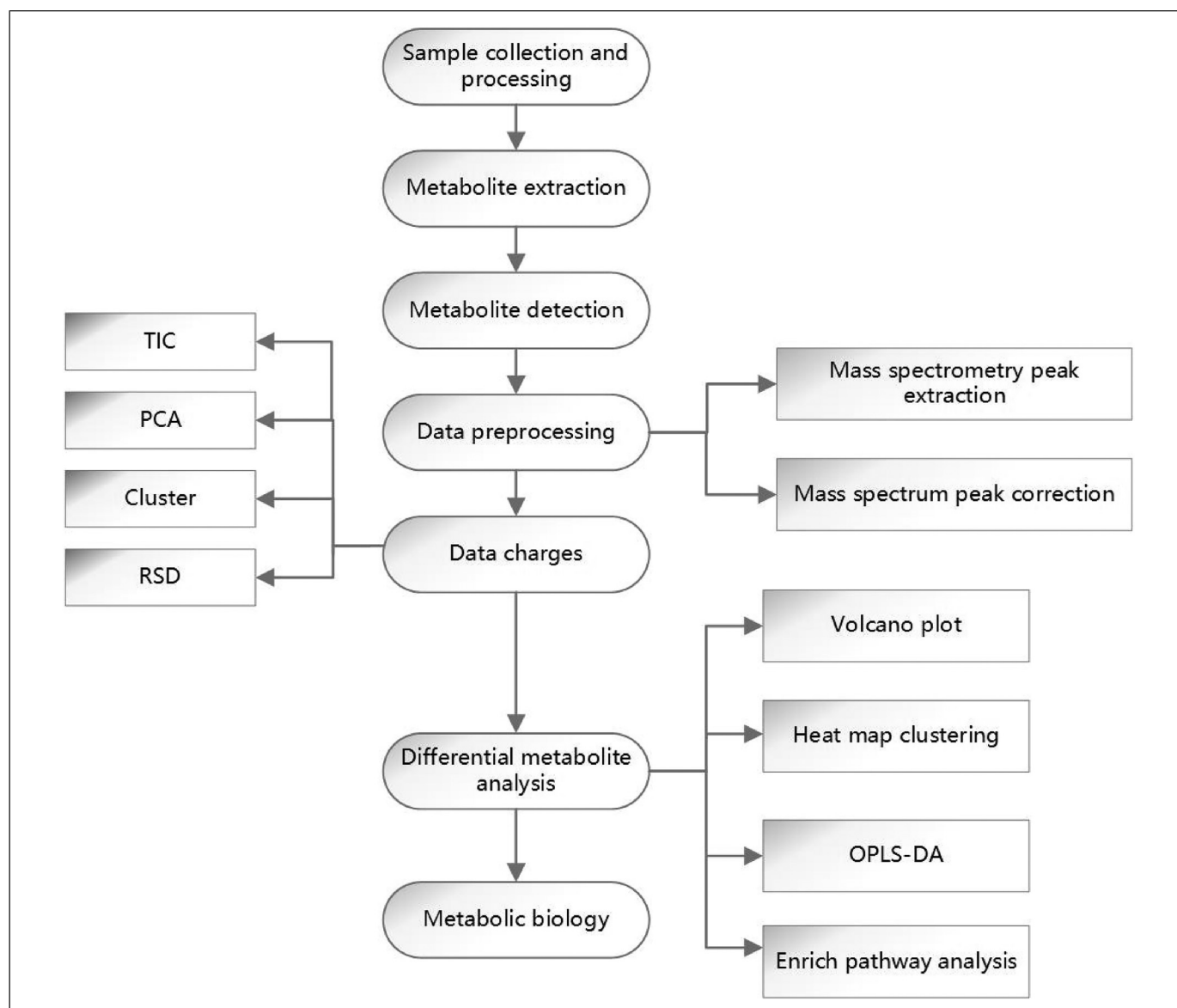


Figure 2. Flow chart of metabolomic analysis.

Screening of Differential Metabolites. Metabonomics data has the characteristics of “high dimension and massive amount,” so it is necessary to combine univariate statistical analysis and multivariate statistical analysis and analyze the data from multiple perspectives according to the characteristics of the data and accurately mine the differential metabolites. Univariate statistical analysis methods include parametric test and nonparametric test. Multivariate statistical analysis methods include PCA, partial least square discriminant analysis, and so on. Based on the results of OPLS-DA, the VIP of the OPLS-DA model was analyzed based on the obtained multivariate data, and the metabolites of different varieties or tissues could be selected preliminarily. At the same time, the P -value or fold change of univariate analysis can be combined to further screen out the differential metabolites. If there is no biological duplicate

sample comparison, difference screening is performed according to fold change value. If there is biological duplication, fold change and VIP values of OPLS-DA model are combined to screen differential metabolites. The metabolites with fold change ≥ 2 and fold change ≤ 0.5 were selected. If the difference of metabolites between the control group and the experimental group is more than 2 times or less than 0.5, the difference is considered significant. If there is biological duplication in the sample grouping, metabolites $VIP \geq 1$ are selected on the basis of the above. VIP value represents the influence intensity of corresponding metabolite differences in the classification discrimination of each group of samples in the model. Generally, $VIP \geq 1$ is considered to have significant differences. Figure 5a shows the VIP values of differential metabolites. The red dots represent up-regulated, while the green dots

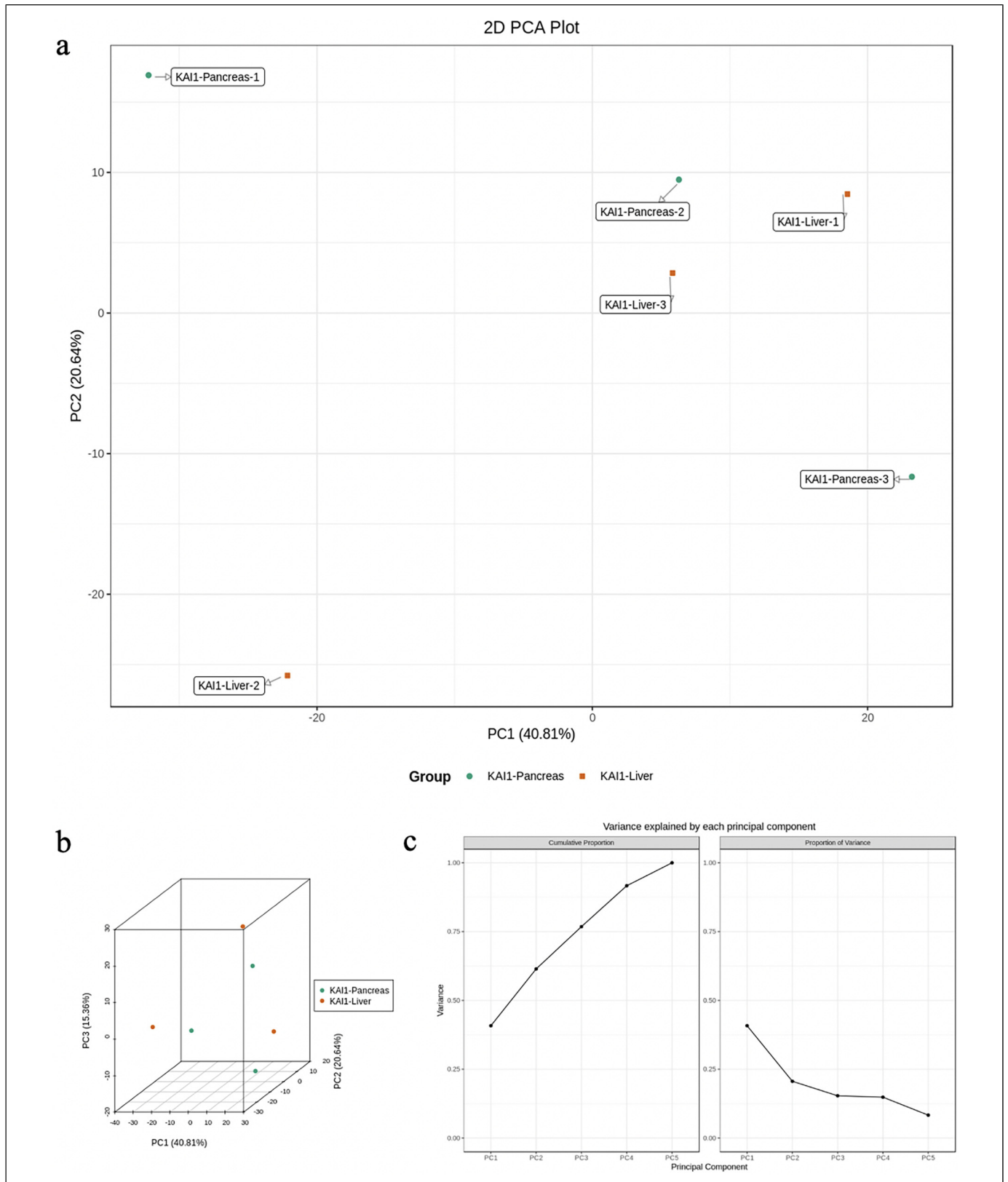


Figure 3. Principal component analysis (PCA) was performed on the samples (including the quality control samples) in order to preliminarily understand the total metabolic differences between the samples of each group and the degree of variation between the samples within the group. (a) PCA 2D results of grouped metabolites. (b) PCA 3D results of grouped metabolites. (c) Explainable variation in the first 5 principal components of PCA. PCA showed a distinct clustering between groups.

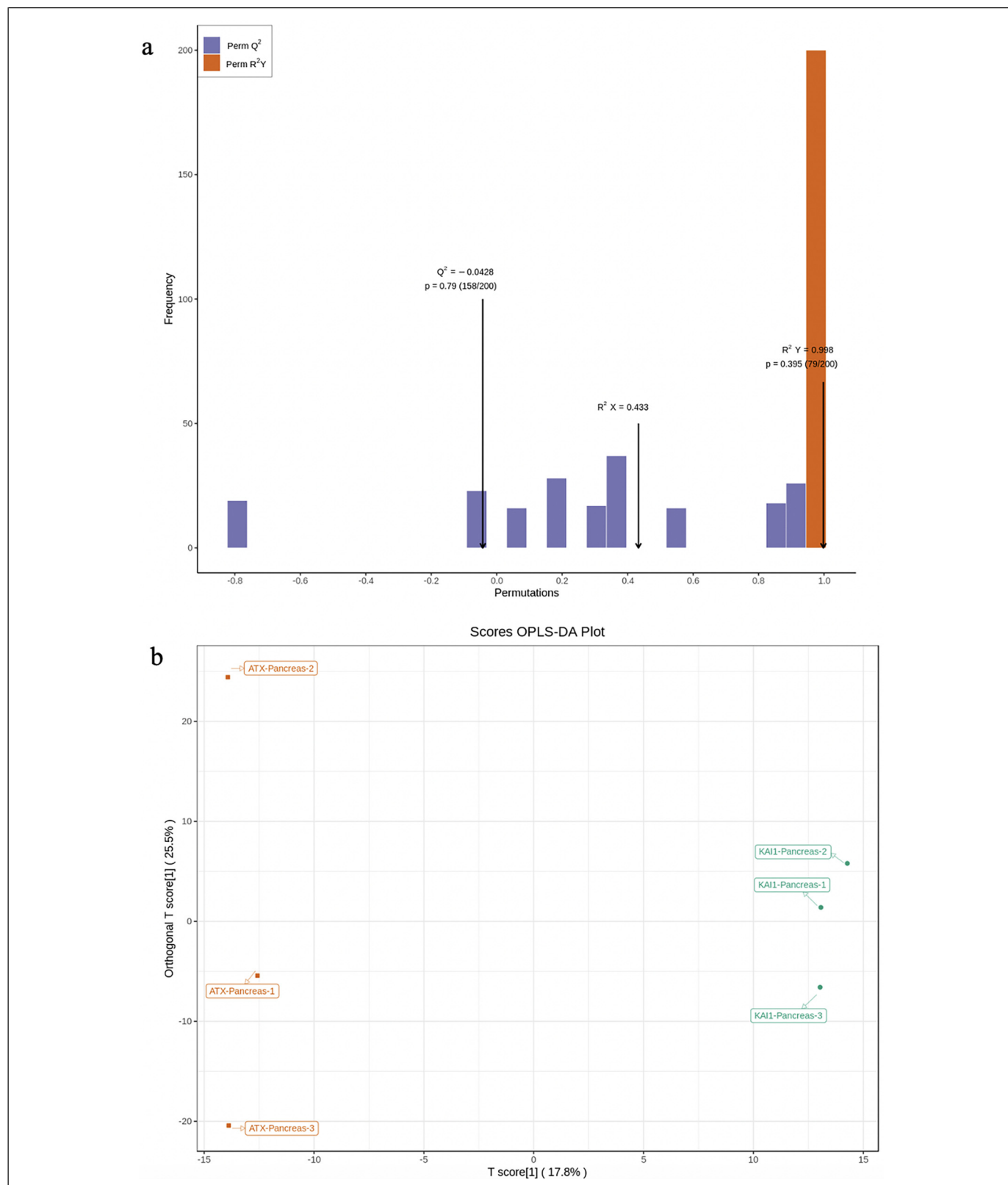


Figure 4. OPLS-DA score plot. (a) OPLS-DA score plot. The abscissa is the difference between groups. The ordinate represents the score value of orthogonal components, and the ordinate direction shows the difference within the group. (b) OPLS-DA model validation. The prediction parameters of the evaluation model include R^2X , R^2Y , and Q^2 . R^2X and R^2Y , respectively, represent the interpretation rate of the established model to the X and Y matrix, and Q^2 represents the prediction ability of the model. The closer these 3 indicators are to 1, the more stable and reliable the model will be.

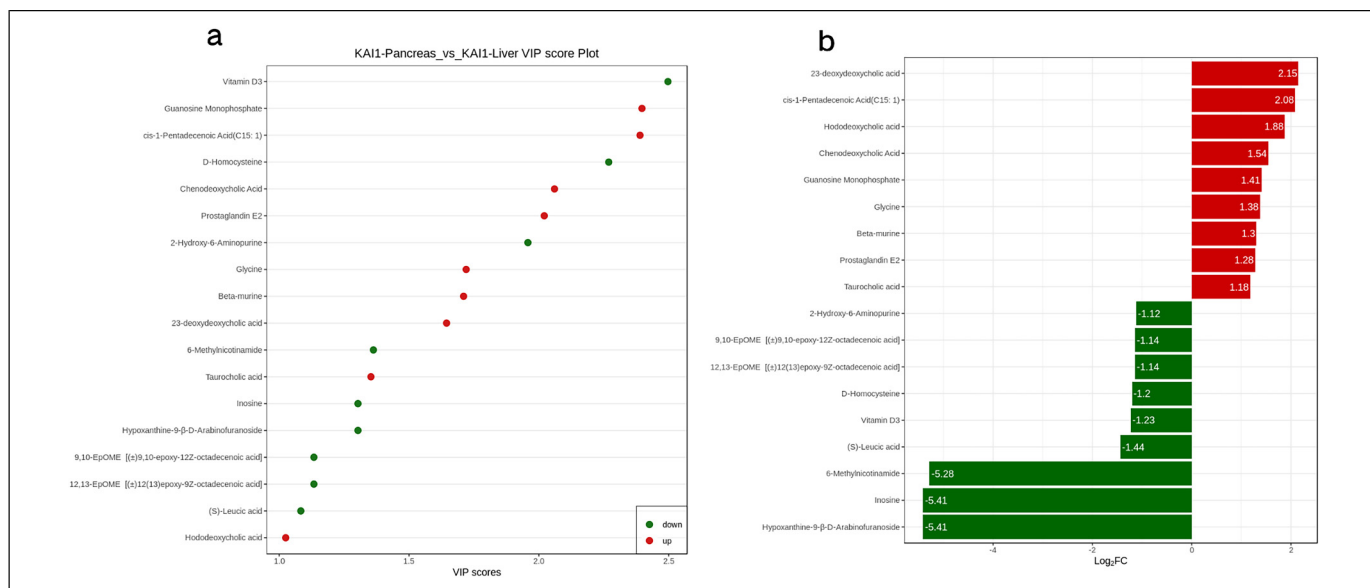


Figure 5. (a) VIP value plot. VIP values of the differentially expressed metabolites. (b) Bar chart. The difference multiple changes of the quantitative information of metabolites in each group were compared according to the grouping of specific samples.

represent downregulated metabolites. After qualitative and quantitative analysis of the detected metabolites, combined with the grouping situation of specific samples, the difference multiple changes of the quantitative information of metabolites in each group were compared. Figure 5b shows the results of metabolites whose changes rank first after log2 processing of the difference multiple in each group comparison. The results of differential metabolite screening are shown in Table 1. Figure 6a is the S-plot of OPLS-DA, where the abscissa represents the cocorrelation coefficient between principal components and metabolites, and the ordinate represents the

correlation coefficient between principal components and metabolites. The closer the metabolites are to the upper right corner and the lower left corner, the more significant the difference is. The red dots indicate the VIP value of these metabolites is greater than or equal to 1. The green dots indicate a VIP value of less than 1 for these metabolites. The volcano plot provides a quick look at the differences in the levels of metabolites expressed in 2 (group) samples and the statistical significance of the differences. Figure 6b presents the metabolite volcano plot, which shows the difference in the metabolite expression level and the statistical significance. The fiddle chart is a

Table 1. Differential Metabolite Screening Results Based on UPLC-MS/MS Platform.

Formula	Compounds	Class	VIP	Log2 ^{FC}	Type
C ₂₆ H ₄₅ NO ₇ S	Taurocholic acid	Bile acids	1.35	1.18	Up
C ₂₄ H ₄₀ O ₄	Hododeoxycholic acid	Bile acids	1.02	1.88	Up
C ₂₄ H ₄₀ O ₄	Chenodeoxycholic Acid	Bile acids	2.06	1.54	Up
C ₁₀ H ₁₄ N ₅ O ₈ P	Guanosine Monophosphate	Nucleotide and its metabolomics	2.40	1.41	Up
C ₂₀ H ₃₂ O ₅	Prostaglandin E2	Hormones and hormone related compunds	2.02	1.28	Up
C ₂₃ H ₃₈ O ₄	23-deoxydeoxycholic acid	Bile acids	1.64	2.15	Up
C ₁₅ H ₂₈ O ₂	cis-1-Pentadecenoic Acid (C15: 1)	FA	2.39	2.08	Up
C ₂ H ₅ NO ₂	Glycine	Amino acid and its metabolomics	1.72	1.38	Up
C ₂₄ H ₄₀ O ₅	Beta-murine	Bile acids	1.71	1.30	Up
C ₂₇ H ₄₄ O	Vitamin D3	CoEnzyme and vitamins	2.50	-1.23	Down
C ₁₀ H ₁₂ N ₄ O ₅	Hypoxanthine-9-β-D-Arabinofuranoside	Nucleotide and its metabolomics	1.30	-5.41	Down
C ₁₈ H ₃₂ O ₃	12,13-EpOME [(±)12 (13) epoxy-9Z-octadecenoic acid]	Oxidized lipids	1.13	-1.14	Down
C ₁₈ H ₃₂ O ₃	9,10-EpOME [(±)9,10-epoxy-12Z-octadecenoic acid]	Oxidized lipids	1.13	-1.14	Down
C ₁₀ H ₁₂ N ₄ O ₅	Inosine	Nucleotide and its metabolomics	1.30	-5.41	Down
C ₆ H ₁₂ O ₃	(S)-Leucic acid	Organic acid and its derivatives	1.08	-1.44	Down
C ₄ H ₉ NO ₂ S	D-Homocysteine	Amino acid and its metabolomics	2.27	-1.20	Down
C ₅ H ₅ N ₅ O	2-Hydroxy-6-Aminopurine	Nucleotide and its metabolomics	1.96	-1.12	Down
C ₇ H ₈ N ₂ O	6-Methylnicotinamide	Heterocyclic compounds	1.36	-5.28	Down

Abbreviations: Class, substance class; Log2^{FC}, the logarithm of fold change is taken as the base of 2; Type, up/down regulated type of metabolite; VIP, projection of variable importance.

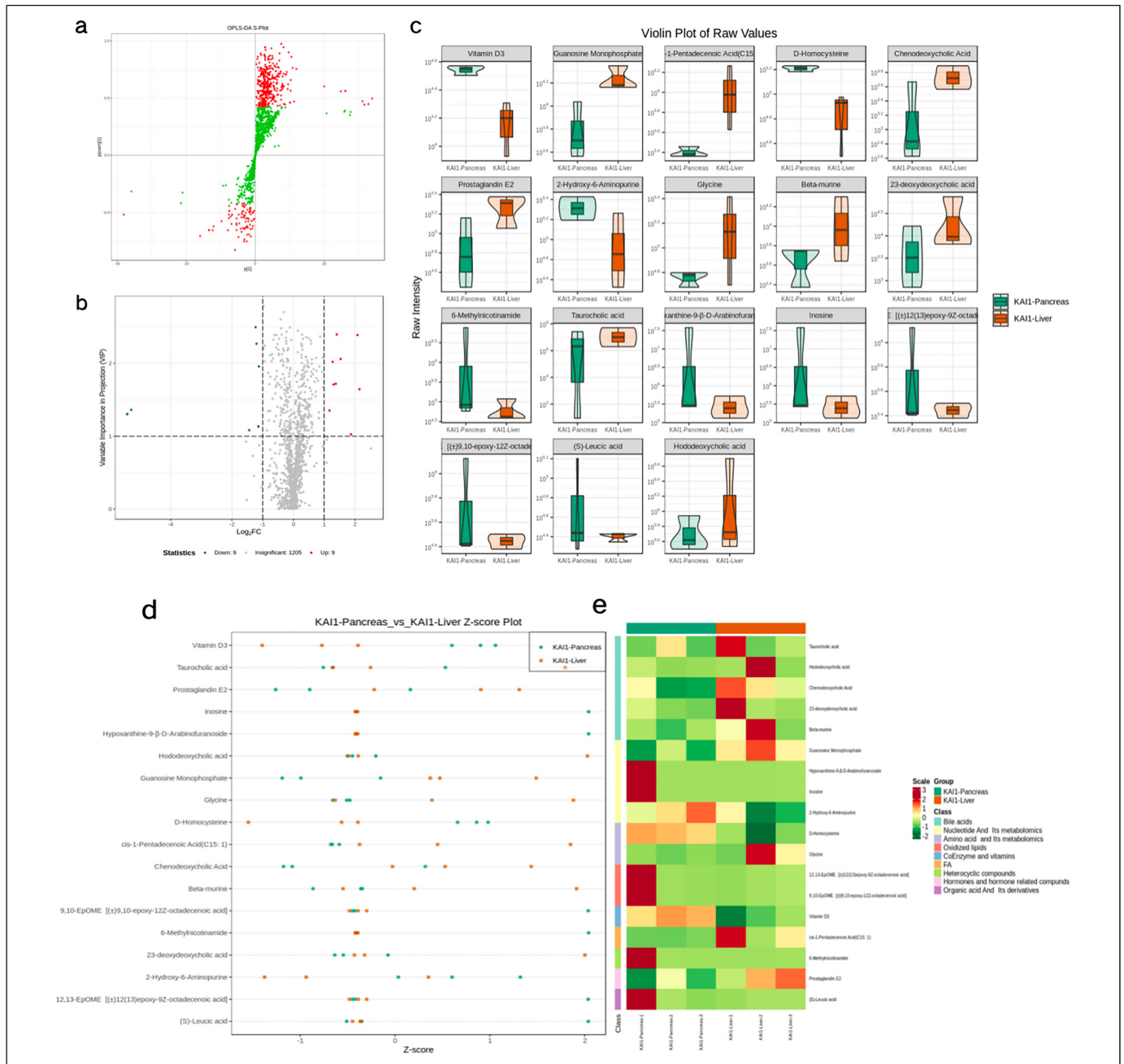


Figure 6. (a) OPLS-DA S-plot. The red points indicate that the VIP value of these metabolites ≥ 1 ; the green points indicate that the VIP value of these metabolites ≤ 1 . The upper right corner or lower left corner metabolites have more significant difference. (b) Volcano plot. Each point in the map represents a metabolite, and the abscisic coordinate represents the logarithm of the quantitative difference multiples of a metabolite in the 2 samples. (c) Violin plot. Violin plot is a combination of boxplot and density map and is mainly used to display the data distribution and its probability density. (d) Z-score plot. The different metabolites in different samples were normalized by calculating the Z-value. The distribution of each differential metabolite between different groups can be distinguished visually. (e). Heatmap clustering. The clustering tree on the left of the figure represents differential metabolites, and the scale represents the expression amount obtained after standardized processing. Abbreviations: OPLS-DA, orthogonal partial least squares discrimination analysis; VIP, variable importance in projection.

combination of a box plot and a density plot which mainly used to show the distribution of data and its probability density. The box in the middle represents the range of quartiles, the thin black line extending from it represents the 95% confidence interval, the black horizontal line in the middle represents the

median, and the outer shape represents the distribution density of data. When the number of differential metabolites exceeded 50, only the top 50 differential metabolites with the highest VIP value were shown, and the results were shown as Figure 6c. Figure 6d shows the Z-score diagram of different

Table 2. KEGG Differential Enrichment Statistics.

KEGG pathway	Com all	Com	<i>P</i>	Uni compounds
Primary bile acid biosynthesis	729	6	2.56×10^{-5}	Taurocholic acid; Glycine; Chenodeoxycholic Acid
Purine metabolism	729	12	2.72×10^{-4}	Inosine; Glycine; Guanosine Monophosphate
Rheumatoid arthritis	729	3	4.04×10^{-4}	Vitamin D3; Prostaglandin E2
Antifolate resistance	729	3	4.04×10^{-4}	D-Homocysteine; Guanosine Monophosphate
Bile secretion	729	34	.006	Chenodeoxycholic Acid; Prostaglandin E2; Taurocholic acid
NOD-like receptor signaling pathway	729	1	.012	D-Homocysteine
Neuroactive ligand-receptor interaction	729	20	.023	Prostaglandin E2; Glycine
Phototransduction	729	2	.024	Guanosine Monophosphate
Olfactory transduction	729	2	.024	Guanosine Monophosphate
Human cytomegalovirus infection	729	2	.024	Prostaglandin E2
cGMP-PKG signaling pathway	729	3	.037	Guanosine Monophosphate
Phosphonate and phosphinate metabolism	729	3	.037	Glycine
Human papillomavirus infection	729	3	.036	Prostaglandin E2
Thiamine metabolism	729	4	.049	Glycine
African trypanosomiasis	729	4	.049	Prostaglandin E2
C-type lectin receptor signaling pathway	729	4	.049	Prostaglandin E2

Abbreviations: Com, the number of metabolites detected that belong to the pathway; Com all, the number of metabolites noted by KEGG in all measured metabolites; *P*, *P* value of hypergeometric distribution; Uni compounds, metabolites that are significantly different and annotated by KEGG.

normalized metabolites in different samples by calculating the *Z* value. Points with different colors represent samples of different groups, and the distribution of each different metabolite among different groups can be seen intuitively. Figure 6e shows the clustering heatmap in order to facilitate the observation of the metabolite changes and normalize the metabolites with significant differences.

Metabolic Pathway and Functional Analysis. As the main public database of relevant pathways, KEGG queries through integrated metabolic pathways (genomes) include the metabolism of carbohydrates, nucleosides, and amino acids and the biodegradation of organisms. Table 2 shows the KEGG differential enrichment statistics. According to the results of differential metabolites, KEGG pathway enrichment was conducted, in which the Rich factor was the ratio of the number of differentially expressed metabolites in the corresponding pathway to the total number of metabolites detected and annotated in the pathway. The size of the points in Figure 7a represents the number of significantly different metabolites enriched to the corresponding pathways. Bile recreation (Figure 8), primary bile acid biosynthesis (Figure 9), and purine metabolism (Figure 10) KEGG pathways contain more differential metabolites that may be associated with liver metastasis from PC.

The human metabolome database (HMDB) is a widely used database, which has collected more than 40 000 endogenous metabolites and information of more than 5000 related proteins (DNA). The database can not only provide links to foreign databases such as KEGG, METLIN, and BioCyc, but also support the retrieval function of mass spectrogram and nuclear magnetic resonance (NMR) spectrogram. The HMDB subdatabase small molecule pathway database also provides an ingenious and detailed description of human metabolism, metabolic disease pathways, metabolite signals, and drug activity pathways. Table 3 shows the HMDB differential enrichment statistics.

According to the enrichment analysis results, the top 20 HMDB primary pathways with *P*-value were selected (considered side by side) for display, in which the Rich factor was the ratio between the number of metabolites in the corresponding pathways differentially expressed and the total number of metabolites detected and annotated by the pathways. The size of the points in Figure 7b represents the number of significantly different metabolites enriched to the corresponding pathways.

Differential Metabolites Associated With Disease. According to KEGG database and HMDB database, the disease information associated with differential metabolites was found. The results are shown in Table 4.

Discussion

PC is estimated to become the second leading cause of cancer-related deaths by 2030 with a 5-year survival rate of only 3% to 5%.²⁶ Thus, new key target genes and the related molecular biological mechanisms for PC need to be explored. In recent years, high-throughput omics techniques have been used as new methods to identify biomarkers related to the pathogenesis of diseases.²⁷ Metabolomic data are high dimensional and massive. Metabolomics analyzes the data from multiple angles according to the data characteristics and identifies the differential metabolites accurately by univariate statistical analysis and multivariate statistical analysis. Untargeted LC-MS has the largest potential to identify novel metabolites due to its increased metabolome coverage.²⁸ Thank you for your valuable suggestions which are very important to our research. Many pure mice (such as C57 or nude mice) are aggressive males, prone to mutual injury and resulting in experimental failure. However, the phenomenon was rare in female mice. Recent studies have shown that the changes of various physiological indexes in female mice during the whole hormonal cycle are

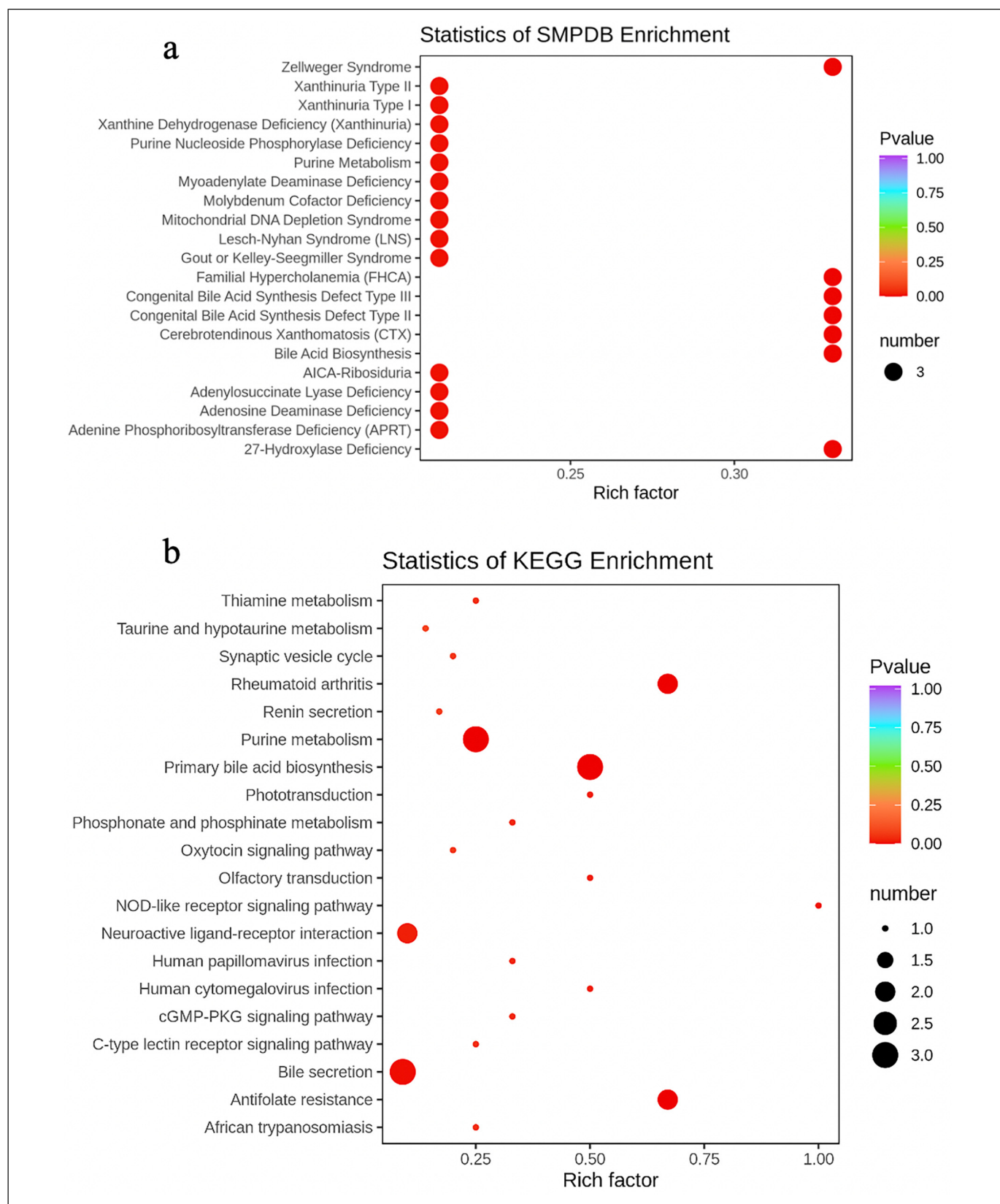


Figure 7. Enrichment analysis. (a) Statistics of KEGG enrichment. (b) Statistics of HMDB enrichment. Rich factor is the ratio between the number of differentially expressed metabolites in the corresponding pathway and the total number of metabolites detected and annotated in the pathway. The size of the points in the figure represents the number of significantly different metabolites enriched to the corresponding pathways. Abbreviations: KEGG, Kyoto encyclopedia of genes and genomes; HMDB, human metabolome database.

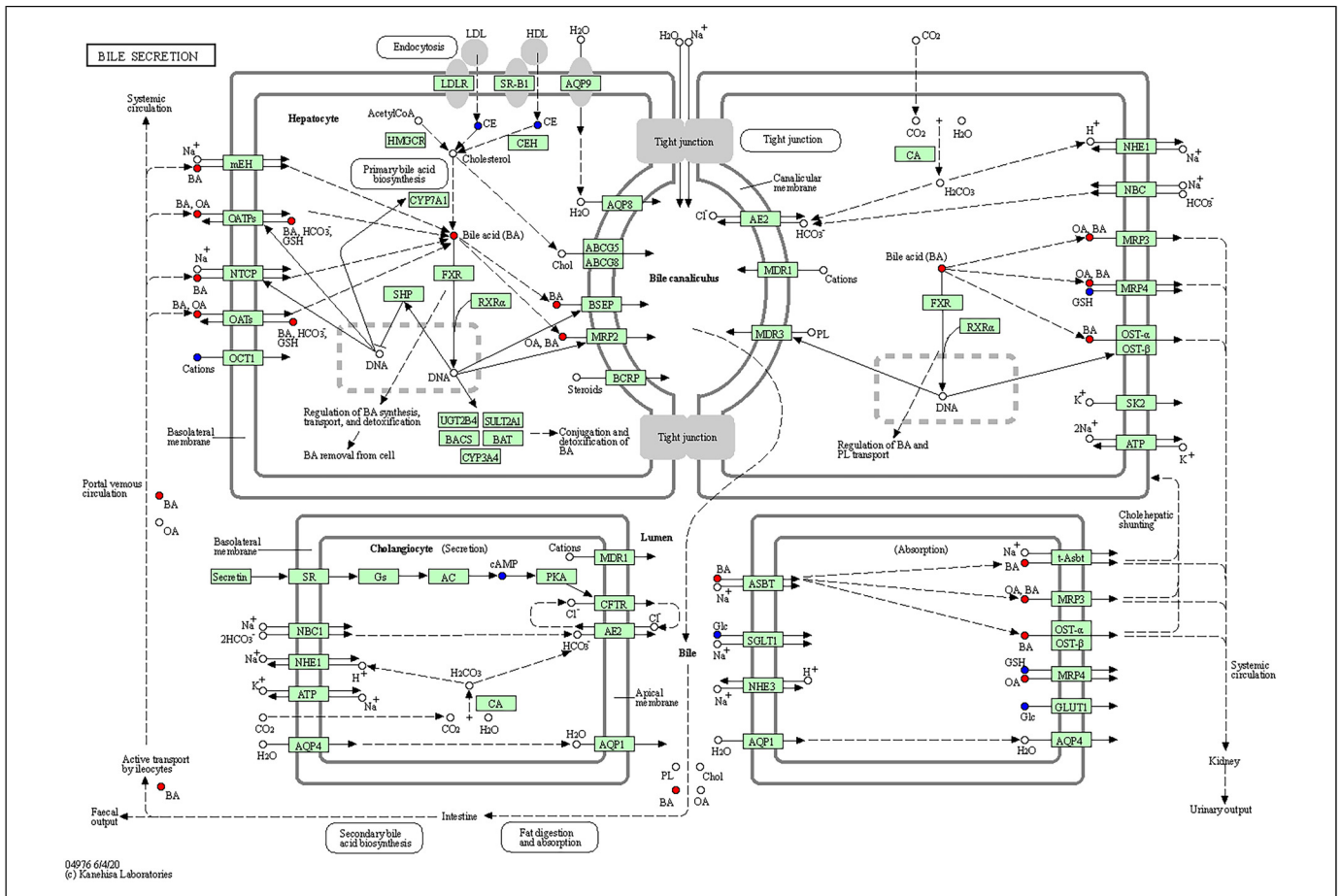


Figure 8. Kyoto encyclopedia of genes and genomes (KEGG) annotation of bile secretion.

no greater than those in male mice and even the individual variation of some sex difference phenotypes in male animals is more obvious than that in female individuals. For example, individual differences in androgen levels will have an impact on tumor treatment. Female nude mice were selected in this study considering that there is no significant difference between male mice and female mice in the individual differences on the formation and metastasis of PC and female mice tend to be raised in groups. Furthermore, there are many previous reports that only female nude mice²⁹⁻³¹ were used in the construction of animal models of malignant tumors. Therefore, female nude mice were selected in this study. In the present study, the serum of PC nude mouse models and liver cancer nude mouse models were analyzed using LC-MS/MS-based metabolomics, which contains 1223 metabolites to discover potential PC liver metastasis biomarkers for diagnosis.

Our research aimed to elucidate the KAI1 regulation mechanism from the perspective of metabolomics. In this study, the KAI1-PLV-EF1α-MCS-IRES-Puro vector and PANC-1 cell lines stably expressing KAI1 were successfully constructed for the first time. The establishment of the nude mouse xenograft model indicated that KAI1 stable expression PANC-1 cell line was feasible, which can function as an *in vivo* mimicking system to explore specific biomarkers of the pathological

process of cancer (eg, metastasis, drug resistance, and hormone-secreting factors). With this function, the nude mouse model allowed us to discover function-oriented biomarkers and identify PC liver metastasis-related serum metabolites. At the same time, the nude mouse model provides pure, stable, and reproducible sample conditions to perform MS analysis, which is a direct successor and modification of former biomarker discovery systems.²³ Ovarian cancer,³²⁻³⁴ hepatocellular carcinoma,³⁵ prostate cancer,³⁶ and lung cancer^{37,38} xenograft nude models have been constructed to search for serum biomarkers. Current studies of PC and metabolomics are mostly conducted in patients with PC and normal controls. However, Coleman et al. utilized patient-derived tumor xenografts to identify patient tumor cell-associated proteins.¹⁸ The purpose of establishing a nude mouse xenograft model was to facilitate the discovery of PC liver metastasis biomarkers. We believe that ongoing animal model-based research will produce a series of comprehensive, pathological process-specific, or personalized biomarkers to distinguish various PC patients, which can meet the increasing clinical needs for precise diagnosis and personalized treatment.

Most cases of PC seem to occur in the head of the gland close to the bile duct, indicating that bile acid may be closely associated with PC.²⁷ Another theory includes bile acid reflux into the pancreas, leading to pancreatitis and eventually malignant cell

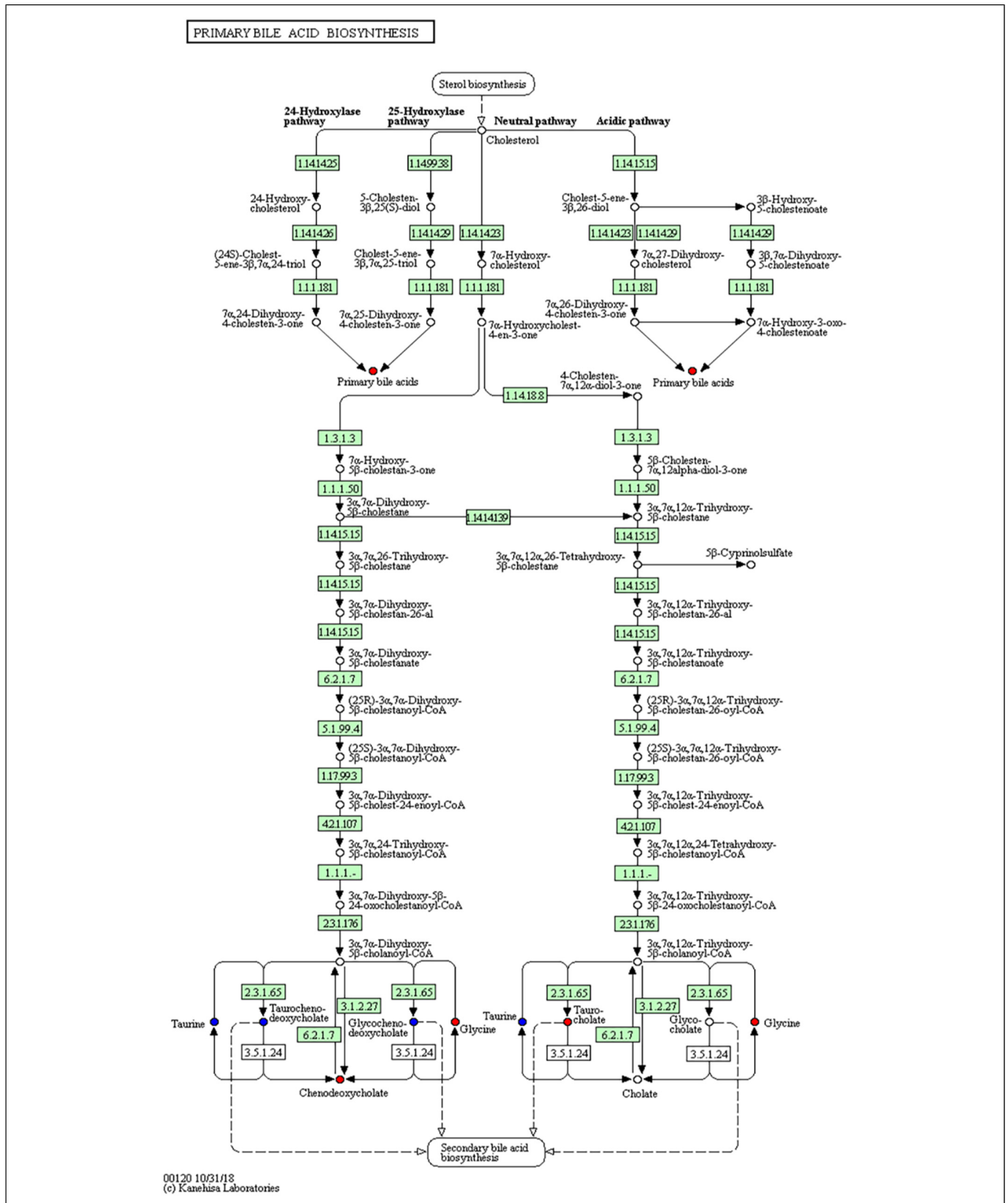


Figure 9. Kyoto encyclopedia of genes and genomes (KEGG) annotation of primary bile acid biosynthesis.

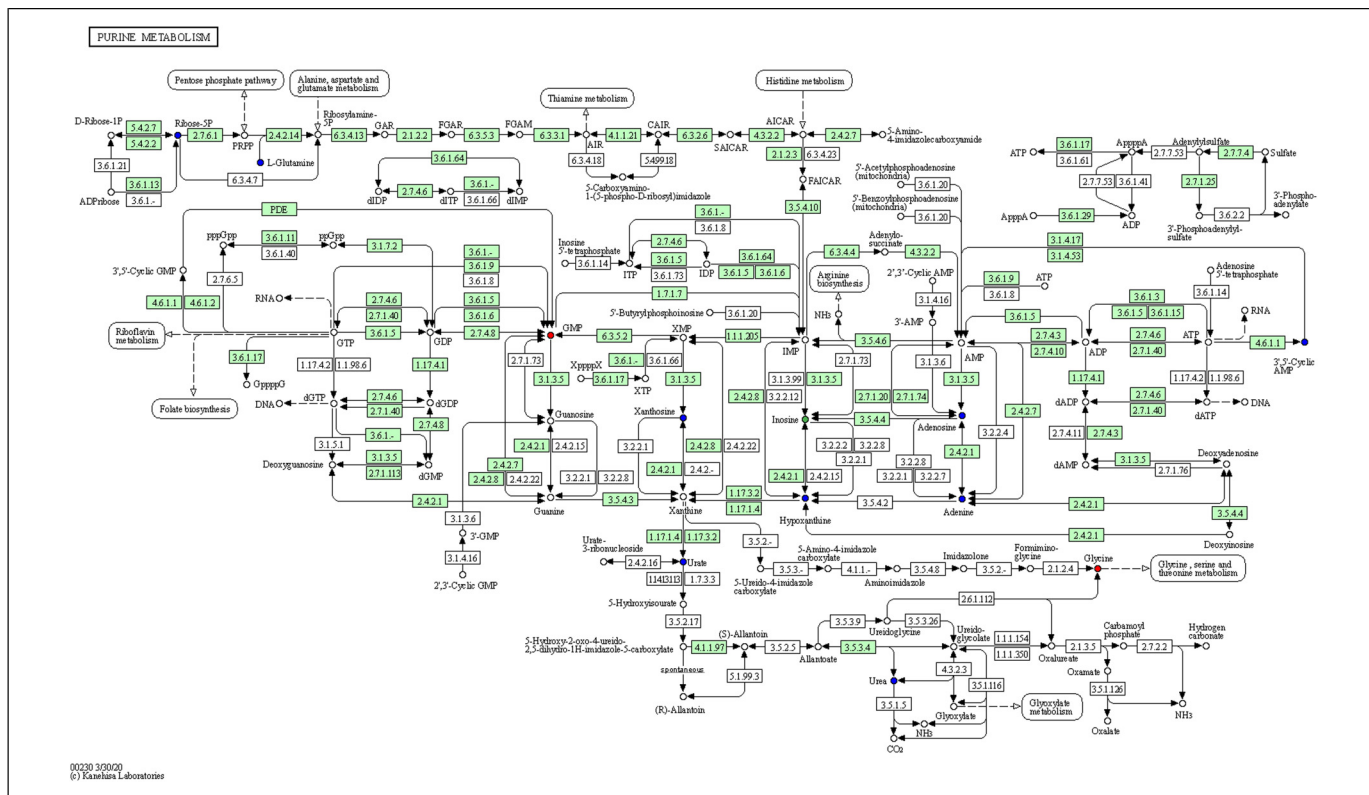


Figure 10. Kyoto encyclopedia of genes and genomes (KEGG) annotation of purine metabolism.

Table 3. HMDB Differential Enrichment Statistics.

SMPDB pathway	N	m	P	Uni compounds
Bile acid biosynthesis	219	9	.002	Taurocholic acid; chenodeoxycholic acid; glycine
Congenital bile acid synthesis defect type III	219	9	.002	Taurocholic acid; chenodeoxycholic acid; glycine
Congenital bile acid synthesis defect type II	219	9	.002	Taurocholic acid; chenodeoxycholic acid; glycine
Cerebrotendinous xanthomatosis (CTX)	219	9	.002	Taurocholic acid; chenodeoxycholic acid; glycine
Zellweger syndrome	219	9	.002	Taurocholic acid; chenodeoxycholic acid; glycine
27-Hydroxylase deficiency	219	9	.002	Taurocholic acid; chenodeoxycholic acid; glycine
Familial hypercholelanemia (FHCA)	219	9	.002	Taurocholic acid; chenodeoxycholic acid; glycine
Xanthine dehydrogenase deficiency (Xanthinuria)	219	14	.010	Guanosine monophosphate; inosine; glycine
AICA-ribosiduria	219	14	.010	Guanosine monophosphate; inosine; glycine
Xanthinuria type I	219	14	.010	Guanosine Monophosphate; Inosine; glycine
Adenosine deaminase deficiency	219	14	.010	Guanosine Monophosphate; Inosine; glycine
Adenylosuccinate lyase deficiency	219	14	.010	Guanosine monophosphate; inosine; glycine
Gout or Kelley-Seegmiller syndrome	219	14	.010	Guanosine monophosphate; inosine; glycine
Molybdenum cofactor deficiency	219	14	.010	Guanosine monophosphate; inosine; glycine
Purine nucleoside phosphorylase deficiency	219	14	.010	Guanosine monophosphate; inosine; glycine
Lesch-Nyhan syndrome (LNS)	219	14	.010	Guanosine monophosphate; inosine; glycine
Myoadenylate deaminase deficiency	219	14	.010	Guanosine monophosphate; inosine; glycine
Mitochondrial DNA depletion syndrome	219	14	.010	Guanosine monophosphate; inosine; glycine
Adenine phosphoribosyltransferase deficiency	219	14	.010	Guanosine monophosphate; inosine; glycine
Purine metabolism	219	14	.010	Guanosine monophosphate; inosine; glycine
Xanthinuria type II	219	14	.010	Guanosine monophosphate; inosine; glycine
Thioguanine action pathway	219	16	.014	Guanosine monophosphate; Inosine; glycine
Mercaptopurine action pathway	219	16	.014	Guanosine monophosphate; inosine; glycine
Azathioprine action pathway	219	16	.014	Guanosine monophosphate; inosine; glycine
tRNA charging: glycine	219	1	.037	glycine
Sarcosine oncometabolite pathway	219	10	.045	D-homocysteine; glycine

Abbreviations: M, the number of metabolites belonging to this pathway in the detected metabolites; N, the number of metabolites annotated by SMPDB primary pathway in all the metabolites measured; P, P value of hypergeometric distribution; Uni compounds, metabolites that are significantly different and annotated by SMPDB.

Table 4. Human Diseases Associated with Differential Metabolites.

Compound name	KEGG diseases	HMDB diseases
Taurocholic acid	–	Hepatocellular carcinoma Cirrhosis Colorectal cancer Crohn's disease Ulcerative colitis Metastatic melanoma Biliary atresia
Chenodeoxycholic acid	–	Cystic fibrosis Biliary atresia Cirrhosis Hepatocellular carcinoma Primary biliary cirrhosis
Glycine	–	D-Glyceric acidemia Refractory localization-related epilepsy Juvenile myoclonic epilepsy Alzheimer's disease D-Glyceric aciduria Early preeclampsia Pregnancy Late-onset preeclampsia 3-Methyl-crotonyl-glycinuria Sarcosinemia N-acetylglutamate synthetase deficiency Histidinemia Obesity Neu-Laxova Syndrome 1 Hyperglycinemia, lactic acidosis, and seizures Pyridoxamine 5-prime-phosphate oxidase deficiency Lipoyltransferase 1 Deficiency Phosphoserine Aminotransferase Deficiency Phosphoserine Phosphatase Deficiency Leukemia Schizophrenia Nonketotic Hyperglycinemia 3-Phosphoglycerate dehydrogenase deficiency Epilepsy, early-onset, vitamin B6-dependent Irritable bowel syndrome Ulcerative colitis Colorectal cancer Autism Crohn's disease Diverticular disease Gout Perillyl alcohol administration for cancer treatment Pancreatic cancer Periodontal disease Frontotemporal dementia Lewy body disease Lung Cancer Carbamoyl Phosphate Synthetase Deficiency Iminoglycinuria Autosomal dominant polycystic kidney disease Argininosuccinic aciduria Propionic acidemia Tyrosinemia I Phenylketonuria Maple syrup urine disease Eosinophilic esophagitis Glucoglycinuria
Prostaglandin E2	–	Amyotrophic lateral sclerosis Hydrocephalus Meningitis
Vitamin D3	Hypercalcemia infantile	Anephric patients Cerebrotendinous xanthomatosis
Guanosine monophosphate	–	–
Inosine	–	Critical illnesses Canavan disease Kidney disease Purine nucleoside phosphorylase deficiency Thymidine treatment Septic shock Xanthinuria type 1 Degenerative disc disease Irritable bowel syndrome Colorectal cancer Crohn's disease Ulcerative colitis Gout Coronary artery disease Attachment loss Periodontal Probing Depth Tooth Decay Eosinophilic esophagitis

transformation. A direct carcinogenic effect of bile acids is also possible. Bile acids are associated with most risk factors of PC, including alcohol intake, smoking, high-fat diet, gallstones, long common channel, chronic pancreatitis, obesity, diabetes, and hypertriglyceridemia. In addition to systemic effects, bile acids have local tissue effects, and they directly activate cancer signaling pathways. Khatun et al.³⁹ and Wolf et al.⁴⁰ discovered that taurocholic acid increases the risk of colon cancer. Chenodeoxycholic acid has been linked to a variety of cancers.⁴¹⁻⁴⁶ In the present study, primary bile acid biosynthesis and bile secretion were not only enriched significantly, but also had more differential metabolites in the KEGG and HMDB pathways, supporting our results and reasoning. Bile acids are likely to be recognized as signaling molecules in liver metastasis of PC in the future.⁴⁷

Among differentially expressed metabolites, amino acids were mostly reported.⁴⁸ Glycine metabolism is thought to be associated with various cancers,^{49,50} including lung cancer,^{51,52} hepatocellular carcinoma,⁵³⁻⁵⁵ colorectal cancer,⁵⁶⁻⁵⁸ and breast cancer.⁵⁹ Some studies have investigated amino acid metabolites in PC.⁶⁰⁻⁶² In our study, glycine was discovered to be metabolically different in the PC and splenic injection liver metastasis models. In recent years, many studies have shown that glycine and its related metabolites and enzymes are closely related to cancer. By observing the changes in the metabolic levels of more than 200 metabolites in more than 60 cell lines, Nilsson

et al. found that glycine consumption and the expression of key enzymes in the glycine biosynthesis pathway in the mitochondria are related to the proliferation rate of cancer cells.⁶³ Excessive activation of the serine/glycine biosynthesis pathway can promote cancer formation. In addition, carbon derivatives from glucose enter the serine/glycine de novo synthesis pathway through glycolysis, followed by the serine/glycine metabolism pathway and folic acid cycle, all of which are closely related to tumor production. Glycine plays a very important role in these pathways. Our analysis results also showed that glycine is the unique compound in various KEGG and HMDB enrichment pathways, which are related to various cancers. KAI1/CD82 may inhibit the expression of glycine and its metabolism to decrease liver metastasis.

As an important inflammatory substance, prostaglandin E2 (PGE2) promotes the occurrence and development of tumors by remodeling the tumor microenvironment. On the one hand, PGE2 can act on immune cells, tumor cells, fibroblasts, and endothelial cells in the microenvironment of PC so as to better support the growth, invasion, and distant metastasis of PC. On the other hand, exosomes released by tumor cells affect the synthesis, release, and uptake of PGE2, improving its ability to reshape the microenvironment. Angiogenesis plays an important role in tumor formation and is involved in tumor energy supply and distant metastasis. Although low

vascular density and highly fibrotic microenvironment are the characteristics of PC, a large number of abnormal vascular endothelial cells are distributed around the tumor in PC tissues.⁶⁴ Cox-2/PGE2 mediates chemotaxis, growth, and aggregation of endothelial cells by regulating the production of proangiogenic factors, such as VEGF, fibroblast growth factor, MMP-9, and integrin.^{65,66} PGE2 can amplify KRAS signal through the positive feedback pathway, both of which are jointly involved in PC intraepithelial neoplasia and are closely related to the EGFR pathway. However, the relationship of PGE2 with KAI1/CD₈₂ remains to be explored.

The relationship between vitamin D and the risk of PC is still controversial, but vitamin D is widely believed to reduce the risk of PC and improve its prognosis. After vitamin E3 binds to its receptor, it can inhibit the growth and proliferation of cells; induce cell differentiation; promote apoptosis, autophagy, antioxidant defense, and DNA damage repair; and inhibit the development of PC by anti-angiogenesis. The 1 α -25(OH)-2-d3 system and VDR can inhibit hypoxia induced by the transcriptional activity of sub-1 (HIF-1) and its target genes (eg, VEGF, ET-1, and Glut-1)⁶⁷ and VEGF protein expression,⁶⁸ which increases the mRNA levels of anti-angiogenesis factors such as platelet response protein-1⁶⁹ and disrupts the IL-8 signaling pathway, thereby inhibiting vascular endothelial cell migration and microvascular formation. However, more research is needed to confirm the antitumor role of vitamin D and its receptor in PC. In addition, vitamin D analogue not only has antitumor activity, but can also overcome the side effects of hypercalcemia. It is expected to be a promising drug for the treatment of PC.

High cGMP levels in pathological samples suggest a strong correlation between intracellular cGMP concentration and carcinoma progression.⁷⁰ The measurement of urinary cGMP levels seems to be a valuable tool in the follow-up of patients with cancer of the uterine cervix,⁷¹ ovarian cancer,^{72,73} gynecological cancer,⁷⁴ gingival cancer,⁷⁵ and colon cancer.^{76,77} GMP synthetase is an important p53 repression target in liver cancer.⁷⁸ It decreases the epithelial markers E-cadherin in breast cancer⁷⁹ and mediates lipopolysaccharide-induced synthesis of Kupffer cell tumor necrosis factor- α .⁸⁰ At present, the signaling pathway of PC remains to be further explored.

Inosine-5'-phosphate dehydrogenase,^{81,82} inosine monophosphate dehydrogenase 2,^{83,84} and inosine 5'-monophosphate dehydrogenase⁸⁵⁻⁸⁷ have a high expression in cancers. Recent bioinformatic analyses fueled by high-throughput sequencing revealed that adenosine-to-inosine RNA editing a widespread modification affecting mostly noncoding repetitive elements in thousands of genes.⁸⁸⁻⁹⁰ Extracellular inosine acts as intermediary in tumor necrosis factor- α stimulated nitric oxide production in cultured Sertoli cells.⁹¹ Inosine can suppress the activity of intracellular lactate dehydrogenase (LDH), thus blocking the major source of energy supply of cancer cells.⁹² Some studies have reported its inhibitory effect on breast cancer,⁹³ liver cancer,⁹⁴ prostate cancer,⁸³ and colon cancer.^{95,96} Although few studies have investigated its mechanism and relationship with PC, inosine is enriched in many metabolic pathways, which may be a new anticancer drug candidate in the future.

Conclusion

We successfully constructed the KAI1-PLV-EF1 α -MCS-IRES-Puro vector and PANC-1 cell lines stably expressing KAI1 for the first time. A series of differentially expressed metabolites and pathways was discovered in PC and liver metastasis nude mouse xenograft models. In agreement with the literature data, the most significant differences between both groups were found in the levels of bile acids (taurocholic acid, chenodeoxycholic acid), glycine, PGE2, vitamin D, GMP, and inosine, as well as the relevant KEGG or HMDB enriched pathways. These findings are expected to improve the prognosis of patients with liver metastasis of PC by aiding the early detection of the disease. Based on the current published literature, we set the sample size as a total of 6. However, the importance of these metabolites on PC liver metastases remains to be elucidated. Hopefully, UPLC-MS/MS-based metabolomics may contribute to the early diagnosis, prevention, and/or therapy of PC in the future.

Authors' Note

Experimental operation, data analysis, and article drafting were completed by Shuo Wang. The project was designed and supervised by Xiaozhong Guo. Parts of the experimental operation and data analysis were completed by Jiang Chen and Hongyu Li. The correction writing and formatting, article revision and review were completed by Xiaozhong Guo, Xingshun Qi, and Xu Liu. All authors read and approved the final manuscript.

Declaration of Conflicting Interests

The authors declared no potential conflicts of interest with respect to the research, authorship, and/or publication of this article.


Funding

The authors disclosed receipt of the following financial support for the research, authorship, and/or publication of this article: This study was supported partly by grants from the National Natural Science Foundation of China (81672465) and the Science and Technology Program of Liaoning Province (2019JH8/10300080).

Ethics Approval

All methods aimed to minimize the suffering of experimental animals were performed in accordance with the animal ethics guidelines and approved by the Ethics Board of China Medical University. The approval number of this animal research was IACUC-001-13.

ORCID iD

Xiaozhong Guo  <https://orcid.org/0000-0002-1418-9305>

References

1. Zhang Q, Zeng L, Chen Y, et al. Pancreatic cancer epidemiology, detection, and management. *Gastroenterol Res Pract*. 2016;2016:8962321.
2. Smith RA, Andrews KS, Brooks D, et al. Cancer screening in the United States, 2017: a review of current American cancer society

- guidelines and current issues in cancer screening. *CA Cancer J Clin.* 2017;67(2):100-121.
3. Ballehaninna UK, Chamberlain RS. Serum CA 19-9 as a biomarker for pancreatic cancer-A comprehensive review. *Indian J Surg Oncol.* 2011;2(2):88-100.
 4. Lee MX, Saif MW. Screening for early pancreatic ductal adenocarcinoma: an urgent call! *Jop.* 2009;10(2):104-108.
 5. Dong JT, Lamb PW, Rinker-Schaeffer CW, et al. KAI1, a metastasis suppressor gene for prostate cancer on human chromosome 11p11.2. *Science.* 1995;268(5212):884-886.
 6. Zhang XA, He B, Zhou B, et al. Requirement of the p130CAS-Crk coupling for metastasis suppressor KAI1/CD82-mediated inhibition of cell migration. *J Biol Chem.* 2003;278(29):27319-27328.
 7. Guo X, Friess H, Graber HU, et al. KAI1 Expression is up-regulated in early pancreatic cancer and decreased in the presence of metastases. *Cancer Res.* 1996;56(21):4876-4880.
 8. Liu X, Guo X-Z, Zhang W-W, et al. KAI1 Inhibits HGF-induced invasion of pancreatic cancer by sphingosine kinase activity. *Hepatobiliary Pancreat Dis Int.* 2011;10(2):201-208.
 9. Liu X, Guo X-Z, Li H-Y, et al. KAI1 Inhibits lymphangiogenesis and lymphatic metastasis of pancreatic cancer in vivo. *Hepatobiliary Pancreat Dis Int.* 2014;13(1):87-92.
 10. Wei Q, Zhang F, Richardson MM, et al. CD82 restrains pathological angiogenesis by altering lipid raft clustering and CD44 trafficking in endothelial cells. *Circulation.* 2014;130(17):1493-1504.
 11. Sridhar SC, Miranti CK. Tetraspanin KAI1/CD82 suppresses invasion by inhibiting integrin-dependent crosstalk with c-Met receptor and Src kinases. *Oncogene.* 2006;25(16):2367-2378.
 12. Tsai YC, Weissman AM. Dissecting the diverse functions of the metastasis suppressor CD82/KAI1. *FEBS Lett.* 2011;585(20):3166-3173.
 13. Fiehn O, Kopka J, Dörmann P, et al. Metabolite profiling for plant functional genomics. *Nat Biotechnol.* 2000;18(11):1157-1161.
 14. Spratlin JL, Serkova NJ, Eckhardt SG. Clinical applications of metabolomics in oncology: a review. *Clin Cancer Res.* 2009;15(2):431-440.
 15. Dunn WB, Broadhurst D, Begley P, et al. Procedures for large-scale metabolic profiling of serum and plasma using gas chromatography and liquid chromatography coupled to mass spectrometry. *Nat Protoc.* 2011;6(7):1060-1083.
 16. Marengo E, Robotti E. Biomarkers for pancreatic cancer: recent achievements in proteomics and genomics through classical and multivariate statistical methods. *World J Gastroenterol.* 2014;20(37):13325-13342.
 17. Pavlova NN, Thompson CB. The emerging hallmarks of cancer metabolism. *Cell Metab.* 2016;23(1):27-47.
 18. Coleman O, Henry M, O'Neill F, et al. A comparative quantitative LC-MS/MS profiling analysis of human pancreatic adenocarcinoma, adjacent-normal tissue, and patient-derived tumour xenografts. *Proteomes.* 2018;6(4):45.
 19. Jiao L, Maity S, Coarfa C, et al. A prospective targeted serum metabolomics study of pancreatic cancer in postmenopausal women. *Cancer Prev Res.* 2019;12(4):237-246.
 20. Zhang X, Shi X, Lu X, et al. Novel metabolomics serum biomarkers for pancreatic ductal adenocarcinoma by the comparison of pre-, postoperative and normal samples. *J Cancer.* 2020;11(16):4641-4651.
 21. He X, Zhong J, Wang S, et al. Serum metabolomics differentiating pancreatic cancer from new-onset diabetes. *Oncotarget.* 2017;8(17):29116-29124.
 22. Lindahl A, Heuchel R, Forshed J, et al. Discrimination of pancreatic cancer and pancreatitis by LC-MS metabolomics. *Metabolomics.* 2017;13(5):61.
 23. Bauden M, Kristl T, Andersson R, et al. Characterization of histone-related chemical modifications in formalin-fixed paraffin-embedded and fresh-frozen human pancreatic cancer xenografts using LC-MS/MS. *Lab Invest.* 2016;97(3):279-288.
 24. Zhu J, He J, Liu Y, et al. Identification of glycoprotein markers for pancreatic cancer CD24+CD44+stem-like cells using nano-LC-MS/MS and tissue microarray. *J Proteome Res.* 2012;11(4):2272-2281.
 25. Jacobs JM, Yoneyama T, Ohtsuki S, et al. Identification of IGFBP2 and IGFBP3 as compensatory biomarkers for CA19-9 in early-stage pancreatic cancer using a combination of antibody-based and LC-MS/MS-based proteomics. *Plos One.* 2016;11(8):e0161009.
 26. Ryder NM, Guha S, Hines OJ, et al. G protein-coupled receptor signaling in human ductal pancreatic cancer cells: neurotensin responsiveness and mitogenic stimulation. *J Cell Physiol.* 2001;186(1):53-64.
 27. Xiong Y, Shi C, Zhong F, et al. LC-MS/MS and SWATH based serum metabolomics enables biomarker discovery in pancreatic cancer. *Clin Chim Acta.* 2020;506:214-221.
 28. Patti GJ, Yanes O, Siuzdak G. Innovation: metabolomics: the apogee of the omics trilogy. *Nat Rev Mol Cell Biol.* 2012;13(4):263-269.
 29. Chen SY, Hu SS, Dong Q, et al. Establishment of paclitaxel-resistant breast cancer cell line and nude mice models, and underlying multidrug resistance mechanisms in vitro and in vivo. *Asian Pac J Cancer Prev.* 2013;14(10):6135-6140.
 30. Das D, Xie L, Wang J, et al. In vivo efficacy studies of novel quinazoline derivatives as irreversible dual EGFR/HER2 inhibitors, in lung cancer xenografts (NCI-H1975) mice models. *Bioorg Chem.* 2020;99:103790.
 31. Zhang X, Chen L, Gao L, et al. Comparative study of the effects of ferrochelataze-siRNA transfection mediated by ultrasound microbubbles and polyethyleneimine in combination with low-dose ALA to enhance PpIX accumulation in human endometrial cancer xenograft nude mice models. *Photochem Photobiol.* 2019;95(4):1045-1051.
 32. He Y, Wu X, Liu X, et al. LC-MS/MS analysis of ovarian cancer metastasis-related proteins using a nude mouse model: 14-3-3 zeta as a candidate biomarker. *J Proteome Res.* 2010;9(12):6180-6190.
 33. Faça VM, Ventura AP, Fitzgibbon MP, et al. Proteomic analysis of ovarian cancer cells reveals dynamic processes of protein secretion and shedding of extra-cellular domains. *PLoS One.* 2008;3(6):e2425.
 34. Gunawardana CG, Kuk C, Smith CR, et al. Comprehensive analysis of conditioned media from ovarian cancer cell lines identifies novel candidate markers of epithelial ovarian cancer. *J Proteome Res.* 2009;8(10):4705-4713.
 35. Li Y, Lin N, Xu J, et al. Measurement of serum and hepatic eicosanoids by liquid chromatography tandem-mass spectrometry (LC-

- MS/MS) in a mouse model of hepatocellular carcinoma (HCC) with delivery of c-Met and activated β -catenin by hepatocyte hydrodynamic injection. *Med Sci Monit.* 2018;24:1670-1679.
36. Lapek JD Jr., Mcgrath JL, Ricke WA, et al. LC/LC-MS/MS of an innovative prostate human epithelial cancer (PHEC) in vitro model system. *J Chromatogr B Analyt Technol Biomed Life Sci.* 2012;893-894:34-42.
37. Beumer JH, Parise RA, Kanterewicz B, et al. A local effect of CYP24 inhibition on lung tumor xenograft exposure to 1,25-dihydroxyvitamin D(3) is revealed using a novel LC-MS/MS assay. *Steroids.* 2012;77(5):477-483.
38. Cang S, Liu R, Wang T, et al. Simultaneous determination of five active alkaloids from compound Kushen injection in rat plasma by LC-MS/MS and its application to a comparative pharmacokinetic study in normal and NSCLC nude rats. *J Chromatogr B Analyt Technol Biomed Life Sci.* 2019;1126-1127:121734.
39. Khatun Z, Nurunnabi M, Reeck GR, et al. Oral delivery of taurocholic acid linked heparin-docetaxel conjugates for cancer therapy. *J Control Release.* 2013;170(1):74-82.
40. Wolf PG, Gaskins HR, Ridlon JM, et al. Effects of taurocholic acid metabolism by gut bacteria: a controlled feeding trial in adult African American subjects at elevated risk for colorectal cancer. *Contemp Clin Trials Commun.* 2020;19:100611.
41. Choi YH, Im EO, Suh H, et al. Apoptosis and modulation of cell cycle control by synthetic derivatives of ursodeoxycholic acid and chenodeoxycholic acid in human prostate cancer cells. *Cancer Lett.* 2003;199(2):157-167.
42. Kim TH, Yoo YH, Kang DY, et al. Efficacy on anaplastic thyroid carcinoma of valproic acid alone or in combination with doxorubicin, a synthetic chenodeoxycholic acid derivative, or lactacystin. *Int J Oncol.* 2009;34(5):1353-1362.
43. Soma T, Kaganoi J, Kawabe A, et al. Chenodeoxycholic acid stimulates the progression of human esophageal cancer cells: a possible mechanism of angiogenesis in patients with esophageal cancer. *Int J Cancer.* 2006;119(4):771-782.
44. Casaburi I, Avena P, Lanzino M, et al. Chenodeoxycholic acid through a TGR5-dependent CREB signaling activation enhances cyclin D1 expression and promotes human endometrial cancer cell proliferation. *Cell Cycle.* 2012;11(14):2699-2710.
45. Yee SB, Yeo WJ, Park BS, et al. Synthetic chenodeoxycholic acid derivatives inhibit glioblastoma multiform tumor growth in vitro and in vivo. *Int J Oncol.* 2005;27(3):653-659.
46. Jeong JH, Park JS, Moon B, et al. Orphan nuclear receptor Nur77 translocates to mitochondria in the early phase of apoptosis induced by synthetic chenodeoxycholic acid derivatives in human stomach cancer cell line SNU-1. *Ann N Y Acad Sci.* 2003;1010:171-177.
47. Feng HY, Chen YC. Role of bile acids in carcinogenesis of pancreatic cancer: an old topic with new perspective. *World J Gastroenterol.* 2016;22(33):7463-7477.
48. Long NP, Yoon SJ, Anh NH, et al. A systematic review on metabolomics-based diagnostic biomarker discovery and validation in pancreatic cancer. *Metabolomics.* 2018;14(8):109.
49. Vong KKH, Tsubokura K, Nakao Y, et al. Cancer cell targeting driven by selective polyamine reactivity with glycine propargyl esters. *Chem Commun (Camb).* 2017;53[60]:8403-8406.
50. Amelio I, Cutruzzolá F, Antonov A, et al. Serine and glycine metabolism in cancer. *Trends Biochem Sci.* 2014;39(4):191-198.
51. Wei HY, Feng R, Shao H, et al. Serum glycine dehydrogenase is associated with increased risk of lung cancer and promotes malignant transformation by regulating DNA methyltransferases expression. *Mol Med Rep.* 2018;18(2):2293-2299.
52. Zhang WC, Shyh-Chang N, Yang H, et al. Glycine decarboxylase activity drives non-small cell lung cancer tumor-initiating cells and tumorigenesis. *Cell.* 2012;148(1-2):259-272.
53. Chen M, Yang MH, Chang MM, et al. Tumor suppressor gene glycine N-methyltransferase and its potential in liver disorders and hepatocellular carcinoma. *Toxicol Appl Pharmacol.* 2019;378:114607.
54. Zhuang H, Wu F, Wei W, et al. Glycine decarboxylase induces autophagy and is downregulated by miRNA-30d-5p in hepatocellular carcinoma. *Cell Death Dis.* 2019;10(3):192.
55. Zhuang H, Li Q, Zhang X, et al. Downregulation of glycine decarboxylase enhanced cofilin-mediated migration in hepatocellular carcinoma cells. *Free Radic Biol Med.* 2018;120:1-12.
56. Oltedal S, Skaland I, Maple-Grødem J, et al. Expression profiling and intracellular localization studies of the novel Proline-, Histidine-, and Glycine-rich protein 1 suggest an essential role in gastro-intestinal epithelium and a potential clinical application in colorectal cancer diagnostics. *BMC Gastroenterol.* 2018;18(1):26.
57. Bruns H, Kazanavicius D, Schultze D, et al. Glycine inhibits angiogenesis in colorectal cancer: role of endothelial cells. *Amino Acids.* 2016;48(11):2549-2558.
58. Terasaki M, Mima M, Kudoh S, et al. Glycine and succinic acid are effective indicators of the suppression of epithelial-mesenchymal transition by fucoxanthinol in colorectal cancer stem-like cells. *Oncol Rep.* 2018;40(1):414-424.
59. Zheng G, Zheng M, Yang B, et al. Improving breast cancer therapy using doxorubicin loaded solid lipid nanoparticles: synthesis of a novel arginine-glycine-aspartic tripeptide conjugated, pH sensitive lipid and evaluation of the nanomedicine in vitro and in vivo. *Biomed Pharmacother.* 2019;116:109006.
60. Tumas J, Kvederaviciute K, Petrulionis M, et al. Metabolomics in pancreatic cancer biomarkers research. *Med Oncol.* 2016;33(12):133.
61. Li MM, Cao J, Yang JC, et al. Effects of arginine-glycine-aspartic acid peptide-conjugated quantum dots-induced photodynamic therapy on pancreatic carcinoma in vivo. *Int J Nanomedicine.* 2017;12:2769-2779.
62. Li MM, Cao J, Yang JC, et al. Biodistribution and toxicity assessment of intratumorally injected arginine-glycine-aspartic acid peptide conjugated to CdSe/ZnS quantum dots in mice bearing pancreatic neoplasm. *Chem Biol Interact.* 2018;291:103-110.
63. Nilsson R, Jain M, Madhusudhan N, et al. Metabolic enzyme expression highlights a key role for MTHFD2 and the mitochondrial folate pathway in cancer. *Nat Commun.* 2014;5:3128.
64. Xu Z, Pothula SP, Wilson JS, et al. Pancreatic cancer and its stroma: a conspiracy theory. *World J Gastroenterol.* 2014;20(32):11216-11229.
65. Rüegg C, Dormond O, Mariotti A. Endothelial cell integrins and COX-2: mediators and therapeutic targets of tumor angiogenesis. *Biochim Biophys Acta.* 2004;1654(1):51-67.

66. Oshima H, Popivanova BK, Oguma K, et al. Activation of epidermal growth factor receptor signaling by the prostaglandin E(2) receptor EP4 pathway during gastric tumorigenesis. *Cancer Sci.* 2011;102(4):713-719.
67. Ben-Shoshan M, Amir S, Dang DT, et al. 1alpha,25-dihydroxyvitamin D3 (Calcitriol) inhibits hypoxia-inducible factor-1/vascular endothelial growth factor pathway in human cancer cells. *Mol Cancer Ther.* 2007;6(4):1433-1439.
68. Lin R, Nagai Y, Sladek R, et al. Expression profiling in squamous carcinoma cells reveals pleiotropic effects of vitamin D3 analog EB1089 signaling on cell proliferation, differentiation, and immune system regulation. *Mol Endocrinol.* 2002;16(6):1243-1256.
69. Fernandez-Garcia NI, Palmer HG, Garcia M, et al. 1alpha,25-Dihydroxyvitamin D3 regulates the expression of Id1 and Id2 genes and the angiogenic phenotype of human colon carcinoma cells. *Oncogene.* 2005;24(43):6533-6544.
70. Di Nicola M, Santoleri F, Soscia S, et al. Cyclic guanosine monophosphate role in human carcinoma pathogenesis. *Nucleosides Nucleotides Nucleic Acids.* 2004;23(8-9):1555-1558.
71. Orbo A, Jaeger R, Sager G. Urinary levels of cyclic guanosine monophosphate (cGMP) in patients with cancer of the uterine cervix: a valuable prognostic factor of clinical outcome? *Eur J Cancer.* 1998;34(9):1460-1462.
72. Luesley DM, Chan KK, Newton JR, et al. Serial urinary cyclic guanosine monophosphate measurements in the assessment of response to treatment in epithelial ovarian cancer. *Br J Obstet Gynaecol.* 1987;94(5):461-466.
73. Luesley DM, Blackledge GR, Chan KK, et al. Random urinary cyclic 3',5' guanosine monophosphate in epithelial ovarian cancer: relation to other prognostic variables and to survival. *Br J Obstet Gynaecol.* 1986;93(4):380-385.
74. Orbo A, Hanevik M, Jaeger R, et al. Urinary cyclic GMP after treatment of gynecological cancer. A prognostic marker of clinical outcome. *Anticancer Res.* 2007;27(4c):2591-2596.
75. Spoto G, Fioroni M, Rubini C, et al. Cyclic guanosine monophosphate phosphodiesterase activity in human gingival carcinoma. *J Oral Pathol Med.* 2003;32(4):189-194.
76. Kwon IK, Schoenlein PV, Delk J, et al. Expression of cyclic guanosine monophosphate-dependent protein kinase in metastatic colon carcinoma cells blocks tumor angiogenesis. *Cancer.* 2008;112(7):1462-1470.
77. Kwon IK, Wang R, Prakash N, et al. Cyclic 3',5'-guanosine monophosphate-dependent protein kinase inhibits colon cancer cell adaptation to hypoxia. *Cancer.* 2011;117(23):5282-5293.
78. Holzer K, Drucker E, Roessler S, et al. Proteomic analysis reveals GMP synthetase as p53 repression target in liver cancer. *Am J Pathol.* 2017;187(2):228-235.
79. Zhang XJ, Zhang WX, Zhu JL, et al. [Effect of cyclic GMP-AMP synthase on EMT in breast cancer cells]. *Zhongguo Ying Yong Sheng Li Xue Za Zhi.* 2020;36(4):336-339.
80. Harbrecht BG, Wang SC, Simmons RL, et al. Cyclic GMP and guanylate cyclase mediate lipopolysaccharide-induced Kupffer cell tumor necrosis factor-alpha synthesis. *J Leukoc Biol.* 1995;57(2):297-302.
81. Collart FR, Chubb CB, Mirkin BL, et al. Increased inosine-5'-phosphate dehydrogenase gene expression in solid tumor tissues and tumor cell lines. *Cancer Res.* 1992;52(20):5826-5828.
82. Jackson RC, Morris HP, Weber G. Partial purification, properties and regulation of inosine 5'phosphate dehydrogenase in normal and malignant rat tissues. *Biochem J.* 1977;166(1):1-10.
83. Wiczorek P, Bałut-Wiczorek M, Jasinski M, et al. Inosine monophosphate dehydrogenase 2 as a marker of aggressive and advanced prostate cancer. *Cent European J Urol.* 2018;71(4):399-403.
84. Chen K, Cao W, Li J, et al. Differential sensitivities of fast- and slow-cycling cancer cells to inosine monophosphate dehydrogenase 2 inhibition by mycophenolic acid. *Mol Med.* 2016;21(1):792-802.
85. Huberman E, Glesne D, Collart F. Regulation and role of inosine-5'-monophosphate dehydrogenase in cell replication, malignant transformation, and differentiation. *Adv Exp Med Biol.* 1994;370:741-746.
86. Szekeres T, Sedlak J, Novotny L. Benzamide riboside, a recent inhibitor of inosine 5'-monophosphate dehydrogenase induces transferrin receptors in cancer cells. *Curr Med Chem.* 2002;9(7):759-764.
87. Floryk D, Thompson TC. Antiproliferative effects of AVN944, a novel inosine 5-monophosphate dehydrogenase inhibitor, in prostate cancer cells. *Int J Cancer.* 2008;123(10):2294-2302.
88. Dominissini D, Moshitch-Moshkovitz S, Amariglio N, et al. Adenosine-to-inosine RNA editing meets cancer. *Carcinogenesis.* 2011;32(11):1569-1577.
89. Paz N, Levanon EY, Amariglio N, et al. Altered adenosine-to-inosine RNA editing in human cancer. *Genome Res.* 2007;17(11):1586-1595.
90. Han J, An O, Hong H, et al. Suppression of adenosine-to-inosine (A-to-I) RNA editome by death associated protein 3 (DAP3) promotes cancer progression. *Sci Adv.* 2020;6(25):eaba5136.
91. De Souza LF, Gelain DP, Jardim FR, et al. Extracellular inosine participates in tumor necrosis factor-alpha induced nitric oxide production in cultured Sertoli cells. *Mol Cell Biochem.* 2006;281(1-2):123-128.
92. Yang X, Hua Y, Zhang X. The cytochemical observation of inosine effect on glucose metabolism of BGC-823 human gastric carcinoma cell line. *Zhonghua Zhong Liu Za Zhi.* 1996;18(1):10-12.
93. Skulchan V, Tantiniti P, Ruangsomboon O, et al. Preventive effect of inosine of leukopenia induced by radiotherapy in breast cancer patients. *J Med Assoc Thai.* 1989;72(9):506-509.
94. Tobólska S, Terpiłowska S, Jaroszewski J, et al. Influence of inosine pranobex on cell viability in normal fibroblasts and liver cancer cells. *J Vet Res.* 2018;62(2):215-220.
95. Lee SH, Kim HP, Kang JK, et al. Identification of diverse adenosine-to-inosine RNA editing subtypes in colorectal cancer. *Cancer Res Treat.* 2017;49(4):1077-1087.
96. Gauthier T, Denis-Pouxviel C, Murat JC. Carbohydrate metabolism in HT29 colon cancer cells cultured in a glucose free medium supplemented with inosine. *Int J Biochem.* 1989;21(2):191-196.